

TITLE

Defense peptides engineered from human platelet factor 4 kill *Plasmodium* by selective membrane disruption

AUTHORS LIST AND AFFILIATIONS

Nicole Lawrence¹, Adelaide S M Dennis², Adele M Lehane², Anna Ehmann³, Peta J Harvey¹, Aurélie H Benfield¹, Olivier Cheneval¹, Sónia Troeira Henriques^{1*}, David J Craik^{1*} and Brendan J McMorran^{3,4*}

¹ Institute for Molecular Bioscience, The University of Queensland, Brisbane, Qld, 4072, Australia

² Research School of Biology, The Australian National University, Canberra, ACT, 2600, Australia

³ The John Curtin School of Medical Research, The Australian National University, Canberra, ACT, 2600, Australia

⁴ Lead Contact

* Correspondence

EMAIL ADDRESSES OF CORRESPONDING AUTHORS

brendan.mcmorran@anu.edu.au

s.henriques@imb.uq.edu.au

d.craik@imb.uq.edu.au

SUMMARY

Malaria is a serious threat to human health and additional classes of antimalarial drugs are greatly needed. The human defense protein, platelet factor 4 (PF4), has intrinsic antiplasmodial activity but also undesirable chemokine properties. We engineered a peptide containing the isolated PF4 antiplasmodial domain, which through cyclization, retained the critical structure of the parent protein. The peptide, cPF4PD, killed cultured blood-stage *Plasmodium falciparum* with low micromolar potency by specific disruption of the parasite digestive vacuole. Its mechanism of action involved selective penetration and accumulation inside the intraerythrocytic parasite without damaging the host cell or parasite membranes; it did not accumulate in uninfected cells. This selective activity was accounted for by observations of the peptide's specific binding and penetration of membranes with exposed negatively-charged phospholipid headgroups. Our findings highlight the tremendous potential of the cPF4PD scaffold for developing antimalarial peptide drugs with a distinct and selective mechanism of action.

Keywords:

host defense, structural biology, drug design, cyclic peptide, membrane lipids, malaria, antiplasmodial, mechanism of action

INTRODUCTION

Malaria is an infectious disease caused by the protozoan parasite, *Plasmodium*, which threatens the lives of more than three billion people from over 90 countries, and which despite control efforts spanning several decades still causes more than 400,000 fatalities annually (Murray et al., 2014; WHO, 2016). Several different classes of antimalarial drugs have been deployed to treat infections and reduce disease incidence. However, in every case, the long-term efficacy of these drugs has been thwarted by the development and spread of drug-resistant strains of the parasite (Haldar et al., 2018). More recently, the use of insecticide-treated bed nets, artemisinin-based combination therapies, and rapid diagnostic tests has resulted in major reductions in malaria incidence in many regions (Bhatt et al., 2015), but the emergence of artemisinin resistance presents a serious threat to the continued success of current control measures (Blasco et al., 2017; Trape et al., 2011). Several small-molecule drugs are progressing toward phase III clinical trials for treating malaria (e.g. OZ439 (McCarthy et al., 2016), KAE609 (White et al., 2014), KAF156 (White et al., 2016), DM265 (Sulyok et al., 2017)). Despite this promise, progress toward the eradication of malaria will require continued development of additional classes of antimalarial drugs that employ alternative mechanisms to target parasites (Wells et al., 2015).

Host defense peptides with antimicrobial activity, collectively termed antimicrobial peptides (AMPs), are produced by a wide variety of organisms (Epanand, 2016; McPhee and Hancock, 2005), and are potentially very useful templates for drug development. The predominant subset of AMPs has a high content of cationic and hydrophobic amino acids and α -helical amphipathic structure. These properties confer the ability to bind

and selectivity target negatively charged microbial membranes over the neutral membranes of healthy eukaryotic cells (Sato and Feix, 2006). After targeting microbial membranes, AMPs act either by disrupting the microbial membrane or by crossing it to gain access to the cytoplasm, where they may inhibit intracellular targets (Yeaman and Yount, 2003).

The membrane of red blood cells (RBCs) infected with *Plasmodium* provides a similar anionic target due to the externalization of phospholipids with negatively-charged phosphatidylserine headgroups onto the outer membrane surface (Eda and Sherman, 2002; Engelbrecht and Coetzer, 2016). In fact, several cationic amphipathic AMPs have been shown to exhibit modest activity against *Plasmodium* blood-stage parasites, albeit with significant hemolytic activity and limited selectivity (Bell, 2011).

Platelet factor 4 (PF4) is a chemokine protein, with antimicrobial properties, that has an AMP-like domain at the C-terminus (Yeaman et al., 2007). It is released by human platelets at high (millimolar) concentrations upon activation (Zucker and Katz, 1991), including in response to *Plasmodium falciparum* infection (Srivastava et al., 2008). It has intrinsic antiplasmodial activity, and treatment of cultured blood-stage *P. falciparum*, the most lethal species of *Plasmodium*, with PF4 significantly inhibits parasite growth (McMorran et al., 2012). The C-terminal, AMP-like domain of PF4 was recently shown to be responsible for this antiplasmodial activity (Love et al., 2012).

PF4 activity and entry into infected RBCs requires initial interaction with the Duffy antigen receptor for chemokines (DARC) on the RBC surface (McMorran et al., 2012). An allelic RBC variant that is common in Africans results in an absence of DARC expression (Howes et al., 2011), and parasites grown in DARC-negative RBCs are

refractory to the killing actions of platelets and PF4 (McMorran et al., 2012). Following entry into infected RBCs, PF4's antimalarial mechanism of action involves disruption of the parasite digestive vacuole (DV) and fragmentation of parasite DNA (Love et al., 2012; McMorran et al., 2012). The antiplasmodial C-terminal domain of PF4 has an amphipathic helical structure with a large proportion of hydrophobic and positively-charged residues, similar to that of some AMPs with high affinity for lipid bilayers and able to target and disrupt anionic microbial cell membranes; thus, the C-terminal domain of PF4 might kill the parasites via a mechanism mediated by interaction with the membranes of infected cells. A small peptide derived from this region (PF4_{C12}) showed modest antiplasmodial activity, and acted via a mechanism similar to that of the full-sized PF4 (Love et al., 2012). However, the large reduction in antiplasmodial potency of PF4_{C12} relative to PF4 suggests that the AMP-like structure of the parent protein domain (required for membrane activity) may not have been achieved for the small peptide.

In striking contrast to all AMPs with antiplasmodial activity described to date, PF4 is unique in its origin from humans. Thus, it represents an unusual opportunity to exploit a self-host defense molecule for developing antimalarial drugs. We reasoned that disadvantages associated with using the full-sized PF4 protein, including non-selective immune regulation that might worsen disease pathology (Srivastava et al., 2010), and inactivity in a DARC-negative host background (McMorran et al., 2012), could be addressed by engineering peptides that isolate and present PF4's antiplasmodial domain in a stabilized configuration.

Here we have successfully harnessed the antiplasmodial activity of PF4 by producing stable, minimized peptides – PF4 peptide dimer (PF4PD) and cyclic PF4

peptide dimer (cPF4PD) – that mimic the essential structure of PF4's AMP-like domain. These peptides represent a great improvement over PF4 and previous PF4-derived peptide analogues, as their potency is similar to the full-sized protein, but they do not contain the N-terminal chemokine domain that is likely associated with undesirable non-specific immune modulation. The minimized cPF4PD peptide achieved the stable α -helical structure that is essential for correctly presenting key charged and hydrophobic residues in an amphipathic arrangement. This stabilized structure resulted in increased membrane binding affinity for anionic phospholipids, which directed selective entry of the peptide into *P. falciparum*-infected RBCs, where it killed parasites by disrupting their DV membrane. These findings demonstrate the great potential of cPF4PD for developing membrane-active peptide drugs to add to the arsenal of weapons in the fight against malaria.

RESULTS

C-terminus of PF4 kills parasites without requiring DARC expression on RBCs

The antiplasmodial potency of full-sized PF4 is highest when DARC is expressed on the surface of RBCs (McMorran et al., 2012). The binding of PF4 to DARC likely increases its concentration at the cell surface and subsequently its rate of internalization. PF4's N-terminus comprises a chemokine sequence (Yeaman et al., 2007) (amino acid positions 1-20 (orange); Figure 1A, 1B) that binds to DARC but is also responsible for the protein's immunomodulatory functions (Srivastava et al., 2010), which are undesirable for drug development. To test if this sequence was expendable for antiplasmodial activity, we generated truncated peptides containing and lacking the

chemokine domain, PF4P₁₋₃₄ and PF4P₃₅₋₇₀, respectively (Figure 1A). The N-terminal chemokine peptide showed no antiplasmodial activity (maximal concentration tested 100 μ M) when used to treat DARC-positive RBCs infected with *P. falciparum*. In contrast, the C-terminal peptide was able to inhibit parasite growth but with an antiplasmodial potency that was ten-fold lower than that of the full-sized PF4 (Figure 1C). These findings confirmed that PF4s C-terminus is required for antiplasmodial activity, but also support our theory that the N-terminal chemokine sequence acts to improve antiplasmodial potency.

To further investigate the dependence on DARC for PF4 potency, we determined the dose response of PF4 against *P. falciparum* cultured in DARC-negative RBCs (Figure 1C, dashed line). The results showed that the full length PF4 is active towards DARC-negative RBCs but lost potency, similar to the decreased potency observed with truncated PF4 peptide (PF4P₃₅₋₇₀), in RBCs containing DARC. The PF4 dose response curve in the DARC-negative cells was notably steeper than in DARC-positive cells, which may indicate different peptide recruitment and entry into each cell type. In an additional set of experiments, *P. falciparum*-infected donor RBCs were treated with PF4 and PF4P₃₅₋₇₀ at concentrations required for 80% inhibition of growth (Figure 1D). At these concentrations, PF4 suppressed the growth of parasites in DARC-positive RBCs (Donor A), but not in DARC-negative RBCs (Donors B, C and D), confirming a DARC-dependent mechanism of action. In contrast, PF4P₃₅₋₇₀ inhibited parasite growth to a similar degree in all of the donor cell types, indicating that the antiplasmodial activity of PF4P₃₅₋₇₀ is DARC-independent, but requires ten-fold higher concentration than the full-length protein.

Together these data confirm that antiplasmodial activity can be achieved by a truncated PF4 C-terminal peptide that does not contain the N-terminal chemokine domain, via a DARC-independent mechanism. Despite the reduction in potency, this mechanism is more advantageous than the DARC-dependent mechanism of full-sized PF4, as it does not discriminate between RBCs from individuals with DARC positive or negative RBCs.

Minimized PF4 C-terminal domain can achieve α -helical conformation as a stable peptide dimer

We hypothesized that the low ($\sim 80 \mu\text{M}$) antiplasmodial potency of the previously reported PF4 C-terminal peptide (PF4_{C12} (Love et al., 2012)), might result from a loss of the AMP-like native structure of the C-terminus of PF4. Within the full-sized protein, this domain has an amphipathic α -helical structure (Figure 1B), where positive residues are located on one side of each helix, and hydrophobic residues on the opposite side. This presentation is known to be important for the activity of AMPs with similar structure, as it promotes interaction with anionic membranes (Yeaman and Yount, 2003).

We prepared a 14-amino acid peptide from the AMP-like C-terminus (Yeaman et al., 2007) of PF4 (PF4P₅₇₋₇₀), and a second peptide consisting of a dimer of the 57-70 region, arranged head-to-tail and separated by a flexible linker sequence (PF4PD). As cyclization often improves the stability and protease resistance of peptides (Chan et al., 2013; Henriques et al., 2017), we also generated a cyclized version of the dimer by introducing a disulfide bridge (cPF4PD). The primary sequence of the PF4-derived peptides is shown in Figure 1A along with the cartoon representation of the full-sized

PF4 (Figure 1B). The predicted structures of PF4P₅₇₋₇₀, PF4PD and cPF4PD are shown in Figure 2A. The mass and purity (>95%) of the synthetic peptides were confirmed by MS and analytical HPLC (see Figure S1, and Table S1 for peptide characteristics).

The overall secondary structure of these three peptides, as well as PF4P₃₅₋₇₀, were examined using circular dichroism (CD) spectroscopy. The results indicated that all four peptides formed α -helical structures in the presence of the hydrophobic solvent trifluoroethanolamine (TFE), indicated by prominent 208 and 222 nm spectral minima (Figure 2B), and relatively high percentage helicities (> 60% for both dimers and the PF4P₃₅₋₇₀ peptide, and 36% for PF4P₅₇₋₇₀; Table S2). For both dimer peptides, the full number of residues predicted to be helix-forming was observed (22/22). In aqueous solution, the 14-amino acid PF4P₅₇₋₇₀ monomer was not helical, whereas the helicities of the other three peptides were maintained to different degrees. The closed cyclic version (cPF4PD) retained the highest proportion of helicity (52%) and number of residues that were predicted to be helical (18/22), whereas PF4PD and PF4P₃₅₋₇₀ were less structured (Figure 2B and Table S2). The different degree of helicity in aqueous solution of cPF4PD versus PF4PD was confirmed by two-dimensional (2D) NMR analysis. Although dispersion was limited, full assignment of backbone resonances of both peptides was achieved (see Figure S2). Secondary alpha proton shifts indicated that PF4PD adopted a random coil structure, whereas two regions of strong helical structure were evident in cPF4PD (Figure 2C). Also, the positioning of helical residues (for example, Leu5-Glu15 and Ala22-Lys31 in cPF4PD) were in agreement with the structure of the AMP-like domain of PF4 (PDB:1F9Q).

Although dimerization of the PF4P₅₇₋₇₀ peptide into the PF4PD open dimer did not greatly enhance its structural stability in aqueous solution, it did provide some resistance to degradation by serum proteases, as the half-life of the dimeric peptide in 25% human serum was increased to 9.0 h, compared to 1.8 h for the unstructured PF4P peptide (Figure 2D). Cyclization of the peptide in the cPF4PD dimer greatly improved both structural stability and resistance to serum proteases, as the rate of proteolysis was very slow ($t_{1/2} \gg 24$ h), with 75% of the closed dimer remaining intact following a 24 h incubation in serum. This stability is an exceptional improvement over the PF4P₅₇₋₇₀ monomer, which was rapidly degraded, with almost no peptide remaining following an 8 h incubation (Figure 2D).

Stabilized PF4 peptide dimers have enhanced antiplasmodial potency

The three minimized PF4 peptides – PF4P₅₇₋₇₀, PF4PD, cPF4PD – were tested for their ability to inhibit the *in vitro* growth of *P. falciparum* cultured in DARC-positive RBCs. Growth inhibition curves revealed that both dimers were potent, with IC₅₀ values of 8.8 μ M for PF4PD and 4.3 μ M for cPF4PD (Figure 3A), whereas the PF4P₅₇₋₇₀ monomer peptide was less active. Notably, the potency of the dimeric peptides was similar to the longer C-terminal peptide (PF4P₃₅₋₇₀, IC₅₀ \sim 5 μ M) and also the potency of the full length PF4 toward DARC-negative infected RBCs.

To examine whether the peptides damaged host RBCs, hemolysis assays were conducted on human RBCs (Figure 3B). The cPF4PD dimer and PF4P₅₇₋₇₀ monomer were non-hemolytic at all of the concentrations tested (up to 64 μ M), whereas PF4PD showed some hemolytic activity at 64 μ M (\sim 20%). In comparison, the control hemolytic

peptide, Melittin (Asthana et al., 2004), induced 100% hemolysis at ~3 μ M. Altogether, these results demonstrate that presenting the minimized PF4 C-terminus in a dimeric peptide scaffold, especially when cyclized (cPF4PD), produces a molecule that is structured and stable in aqueous solution, resistant to serum proteases, non-hemolytic, and able to specifically inhibit the *in vitro* growth of *P. falciparum*.

The mechanism of cPF4PD action against *P. falciparum* involves DV lysis and parasite DNA fragmentation

To examine whether the minimized peptides followed the same mechanism of action as the full-sized PF4 against *P. falciparum* parasites, we prepared a labeled cyclized PF4P dimer peptide with Alexa Fluor 488 (cPF4PD-A488) and confirmed the incorporation of a single A488 probe that did not alter membrane-binding properties (Table S1, Figure S3). The interaction of cPF4PD-A488 with parasitized and uninfected cells was quantified using flow cytometry, and the intracellular location was visualized using fluorescence microscopy. Flow cytometric analysis of RBCs (DARC-positive) treated with increasing peptide concentrations indicated that cPF4PD-A488 uptake was dose dependent and that trophozoite stage (mature) parasites internalized approximately 4-fold greater amounts of peptide than ring stage (immature) parasites, whereas uptake into uninfected cells was virtually undetectable (Figure 3C). Examination of the treated cells by fluorescence microscopy confirmed the relative differences in amounts of peptide in trophozoite versus ring stage parasites, and its absence in uninfected cells (Figure 3D). Remarkably, cPF4PD-A488 was observed inside the parasite but not in the surrounding host cell cytoplasm. To further study this

phenomenon, parasites treated with cPF4PD-A488 were examined using a combination of DIC imaging and immunostaining to detect the parasite parasitophorous vacuole membrane (PVM) protein, *PfExp2* (de Koning-Ward et al., 2009). These results indicated that the RBC plasma membrane and parasite PVM were apparently undamaged by the peptide treatment, and confirmed that the peptide was restricted to within the parasite cytosol (Figure 3E). Therefore, despite the absence of the chemokine sequence from full-sized PF4, the minimized cPF4PD peptide was able to enter RBCs infected with *P. falciparum* and translocate into the parasite cytosol. It did not enter uninfected RBCs, which further improves the safety profile for cPF4PD.

To further characterize the antiplasmodial mechanism of action of cPF4PD, we investigated its effects on RBCs infected with a *P. falciparum* strain expressing GFP-tagged Plasmeprin II (Klonis et al., 2007), which is normally present in the DV of healthy parasites, but redistributes into the parasite cytosol if DV membrane integrity is disrupted (Love et al., 2012). We also conducted terminal deoxynucleotidyl transferase dUTP nick end labelling (TUNEL) on treated and untreated cells to detect parasites with fragmented DNA, which identifies them as dead or dying (McMorran et al., 2009). Thus, we could observe (Figure 4A) and quantify (Figure 4B) parasites with lysed DV, and that were either alive (TUNEL-) or dead (TUNEL+), following different incubation times with the peptide (ranging from 1.5 to 9 h). A proportion of parasites in the untreated group showed DV lysis (20 - 25%), and some of these were dead; however, there was a minimal increase in their number over the period of incubation. In contrast, DV lysis was observed in 50 - 70% of the parasites treated with cPF4PD, and the proportion of those that were also TUNEL+ increased during the incubation period, from ~50% after 1.5 h to

>80% after 9 h. These observations demonstrate that the antiplasmodial mechanism of cPF4PD is similar to that previously described for the PF4 protein (Love et al., 2012), and provide an important causal link between DV lysis and parasite death.

As a complementary and more directed approach to investigate the apparent effects of cPF4PD on the parasite DV (pH_{DV}), we employed an assay to detect disturbances in the intra-organelle pH, which is maintained in the range $\sim 5 - 5.5$ (Hayward et al., 2006; Klonis et al., 2007; Kuhn et al., 2007), primarily through the action of the V-type H^+ -ATPase on the DV membrane (Saliba et al., 2003). Measurements of pH_{DV} were performed using trophozoite-stage parasites that had been functionally isolated from their host cells using saponin, and contained a membrane-impermeant pH-sensitive dye (fluorescein-dextran) in their DVs. The ratio of the fluorescence obtained following excitation of the cell suspension at two wavelengths (the pH-sensitive numerator (495 nm) and the pH-insensitive denominator (440 nm)) provides an indicator of pH_{DV} . Addition of cPF4PD to parasite suspensions caused a gradual, immediate-onset of alkalinization of the DV. The effect of cPF4PD on pH_{DV} was dose dependent, and at $12.5 \mu\text{M}$ (the highest concentration tested) the magnitude of the increase in fluorescence ratio observed was comparable to that resulting from addition of the V-type H^+ -ATPase inhibitor concanamycin A (Con A; $0.1 \mu\text{M}$) (Figure 4C).

We also investigated the effect of cPF4PD on parasite cytosolic pH (pH_i), using isolated trophozoite-stage parasites loaded with the pH-sensitive dye 2',7'-bis-(2-carboxyethyl)-5-(and-6)-carboxyfluorescein acetoxymethyl ester (BCECF). pH_i is regulated by the V-type H^+ -ATPase (which localizes to the parasite plasma membrane in addition to the DV membrane) and is maintained at ~ 7.3 (Saliba and Kirk, 1999).

Addition of 1 μM or 4 μM cPF4PD did not cause any significant change to the pH_i , whereas the addition of the positive control Con A induced a cytosolic acidification (Figure 4D). Together, these results indicate that following treatment with cPF4PD, maintenance of pH_{DV} is disrupted, probably as a result of damage to the DV membrane that renders it unable to maintain ion gradients. However, the parasite is able to maintain a normal pH_i , suggesting that its plasma membrane remains intact and that the plasma membrane V-type H^+ -ATPase remains operational.

Preferential binding to anionic membranes contributes to selectivity and activity against RBCs infected with *P. falciparum*

To determine whether differences in the phospholipid composition of uninfected and infected RBC membranes, and also parasite membranes, plays a role in the selective binding, entry and membrane disruption by the dimeric and monomer PF4-peptides, we studied their affinity for lipid bilayers composed of mixtures of neutral and anionic phospholipids.

The membranes of uninfected RBCs were represented by neutral model membranes composed of pure palmitoyl-2-oleoyl-sn-glycero-3-phosphocholine (POPC) and of a mixture of POPC with cholesterol (Chol) and sphingomyelin (SM; POPC/Chol/SM (2.7:3.3:4) molar ratio). POPC mimics properties of the outer leaflet of mammalian cell membranes, which are fluid and rich in zwitterionic phospholipids containing phosphatidylcholine (PC)-headgroups. POPC/Chol/SM was used to mimic raft-like domains (i.e., regions in the cell membrane where Chol and SM segregate and form domains with liquid-ordered properties, more rigid than the overall fluid

membrane), which are also present in the outer leaflet of RBC membranes (Mikhalyov and Samsonov, 2011; Salzer and Prohaska, 2001).

The membrane of *Plasmodium*-infected RBCs was represented by mixtures of POPC with 1-palmitoyl-2-oleoyl-sn-glycero-3-phosphoserine (POPS; POPC/POPS), as phospholipids with phosphatidylserine (PS)-headgroups are exposed on the outer surface of infected RBCs (Eda and Sherman, 2002; Engelbrecht and Coetzer, 2016). The effect of increasing the proportion of charged lipids was examined using mixtures of POPC/POPS with 4:1 and 3:2 molar ratios. Parasite organellar membranes have a high proportion of anionic phospholipids and two additional mixtures of POPC with anionic phospholipids have been included to represent these: POPC with palmitoyl-2-oleoyl-sn-glycero-3-phosphoglycerol (POPG; POPC/POPG (4:1 molar ratio)) for the parasite mitochondrial membrane (high proportions of phospholipids with phosphatidylglycerol (PG)-headgroups (Schenkel and Bakovic, 2014)); and POPC with L- α -phosphatidylinositol (PI; POPC/PI (4:1 molar ratio)) for the DV membrane (contains phospholipids with PI-headgroups (Tawk et al., 2010)).

All three minimized peptides, PF4P₅₇₋₇₀, PF4PD and cPF4PD bound to the anionic model membrane POPC/POPS (4:1) with higher affinity than to the neutral POPC model membrane (Figure 5A). The rate of peptide association with the POPC/POPS (4:1) model membrane was rapid, with a slower dissociation (Figure 5B), and increasing the proportion of POPS in the mixture (POPC/POPS, 3:2) resulted in higher affinity binding for cPF4PD (Figure 5C). These differences in binding are consistent with the internalization of the cPF4PD peptide into infected RBCs (PS on surface), particularly those infected with more mature trophozoite stage parasites

(Figure 3C, 3D), as the proportion of PS on the RBC surface increases (Sherman et al., 2004), but not into uninfected RBCs (neutral surface). The binding affinity of cPF4PD was similar for all phospholipid mixtures with the same proportion of anionic headgroups (4:1), suggesting that peptide binding is dependent on the overall negative charge at the membrane surface, regardless of the anionic headgroups tested: PS, PG, PI (Figure 5C). Peptide binding to both neutral model membranes, the more rigid POPC/Chol/SM and the fluid POPC, was of similarly weak affinity compared to all of the anionic mixtures (Figure 5C).

The ability of PF4-derived peptides to disrupt anionic and neutral model membranes was examined with carboxyfluorescein (CF)-loaded phospholipid vesicles and quantified by increase in the fluorescence emission intensity of CF upon membrane disruption and leakage of CF. Figure 5D shows that the peptides disrupted negatively-charged POPC/POPS (4:1) membranes with much higher efficiency than neutral POPC membranes. The peptide concentration required to permeabilize 50% of the 5 μ M POPC/POPS (4:1) vesicles (PC_{50}) was 0.02 μ M for PF4PD (P/L, 0.004 mol/mol), 0.06 μ M for cPF4PD (P/L, 0.01 mol/mol), and 1.5 μ M for PF4P₅₇₋₇₀ (P/L, 0.3 mol/mol). The trend in disruption efficiency of PF4PD > cPF4PD >> PF4P₅₇₋₇₀ was consistent with the binding affinities observed with SPR. For all three peptides, neutral POPC vesicles were permeabilized much less efficiently, with > 100-fold higher peptide concentrations required to induce CF-leakage. Overall, leakage of negatively-charged membranes and not of neutral, correlated with the lower binding affinities for POPC membranes observed via SPR, and was consistent with the higher degree of lysis for more

negatively charged parasite organelle membranes, and not of the host membrane of infected RBCs or uninfected RBCs, which are both less negative.

DISCUSSION

Developing antimalarial drugs that employ different and selective mechanisms of action will increase the arsenal of weapons against the lethal *P. falciparum* parasite. In the current study, we successfully minimized the antiplasmodial C-terminal domain of the human defense protein PF4 to generate a stable and structured cyclic peptide – cPF4PD. Our lead peptide has promising antiplasmodial activity with low micromolar potency similar to the full-sized PF4 protein.

Minimizing PF4 peptides to remove the N-terminal chemokine sequence successfully negated the requirement for DARC expression on RBCs for activity, and it is anticipated that undesirable non-specific immune modulation will also be reduced. We demonstrated that the α -helical structure of PF4's C-terminal domain is required for antiplasmodial activity, and we maintained antiplasmodial potency by stabilizing PF4's minimal C-terminal domains in a cyclized head-to-tail dimer. This allowed the peptide to achieve structural stability, in the absence of the larger proteins quaternary structure, and also afforded resistance from serum proteases *in vitro*. Further pharmacokinetic studies and intestinal permeability studies would be required to determine whether this stability translates to *in vivo* stability and bioavailability, and modifications including conjugation to polyethylene glycol or to auxiliary peptides that bind serum proteins (Pollaro et al., 2015), may be required to optimize the peptides for *in vivo* application.

Like the full-sized PF4 protein, cPF4PD is able to selectively target and enter into RBCs infected with *P. falciparum*, either via an endocytic pathway and/or direct membrane permeation, but not into uninfected cells. Internalization of the peptide does not appear to require recruitment at the cell surface through receptor (DARC) binding. cPF4PD is potent in the low micromolar range and kills malaria parasites by disrupting the intracellular parasite DV membrane, without damaging the RBC membrane of infected or uninfected cells. Selective entry into infected RBCs by the cPF4PD peptide, and subsequent activity against intracellular *Plasmodium*, is probably achieved through binding to anionic phospholipid headgroups presented on the surface of host RBC and parasite membranes. RBCs infected with *P. falciparum* present PS-phospholipids on the outer leaflet of the cell membrane, providing a therapeutic target for the Lys-rich cPF4PD peptide. Increasing the proportion of negatively charged phospholipids in model lipid bilayers also increased the affinity of binding by cPF4PD, and this explains the differential activity of the peptide whereby binding, penetration or disruption of host and parasite membranes is dependent on the proportion of anionic phospholipids. For example, the parasite DV membrane, which is lysed by cPF4PD, contains phosphorylated PI-headgroups (Tawk et al., 2010), which contribute to a higher overall negative charge than the host RBC membrane and parasite plasma membrane, which are not lysed.

cPF4PD is a unique antimalarial peptide lead, derived from a human host defense protein. It is potent in the low micromolar range, is not hemolytic up to 64 μ M and has a selective membrane-dependent mechanism of action that is distinct from other small molecule drugs and AMPs. The membrane selectivity also affords cPF4PD

a higher therapeutic index than other AMPs with micromolar antimalarial activity (Bell, 2011; Vale et al., 2014). For example, dermaseptin (from the skin of *Phyllomedusa* frogs) analogues with high potency against blood stage *P. falciparum* (IC₅₀ 0.2 - 1 μM) show >20% hemolysis at 1 μM (Ghosh et al., 1997; Krugliak et al., 2000). It is extremely important that RBC lysis is minimized for prospective antimalarial therapeutics to avoid worsening of anemia, which is a significant contributor to malaria disease pathology (Totino et al., 2010).

Due to the intrinsic selectivity of cPF4PD for infected RBCs and its ability to enter *Plasmodium* parasites without damaging host cells, the stable cyclic peptide is a strong candidate as a scaffold for targeting key intracellular *Plasmodium* pathways. This potential can be realized by incorporating amino acid modifications and/or including a desired sequence into the peptide framework, as has been previously shown for a range of therapeutic applications (reviewed by (Craik and Du, 2017)). For example, a short sequence that blocks the p53 tumor suppressor pathway was included in the cyclotide MCoTi-I. The resultant peptide was able to enter cancer cells and activate the p53 pathway, causing cell death *in vitro* and *in vivo* (Ji et al., 2013).

The history of rapid development of resistance to antimalarial drugs spans several decades, and the prospect of emerging resistance to artemisinin-based combination therapies presents a dire forecast for increased annual deaths (Blasco et al., 2017; Lubell et al., 2014). The report of multiple independent K13 gene mutations that confer artemisinin resistance in southeast Asia (Takala-Harrison et al., 2015) provides strong evidence that the need to develop drugs that employ alternative mechanisms of action is ongoing and great.

The development and delivery of antimalarial drugs also needs to be affordable for uptake by countries with the poorest economic status, often those most ravaged by the disease. The ability to produce a stable, structured and active antimalarial lead using natural amino acids is a significant achievement that complements, but represents an alternative approach to the previous development of small molecule mimetics from PF4 (e.g. PMX207, PMX1207) (Love et al., 2012). In contrast to synthetically modified small molecule drugs, peptide-based drugs composed of natural amino acids can be produced via less expensive synthetic chemistry or recombinant expression approaches.

In conclusion, we have generated an antimalarial peptide lead that is active against *P. falciparum* at therapeutically relevant concentrations. cPF4PD is selective for infected RBCs and has a high window of safety due to its minimal hemolytic activity. The differential membrane-active properties of cPF4PD represents an alternative mechanism of action compared to small molecule drugs. The cPF4PD peptide is minimized to capture antiplasmodial activity, while avoiding undesirable non-specific activity of larger host defense proteins. The stable peptide framework, based on natural amino acids, provides options for low cost manufacture and also the possibility of targeting key intracellular *Plasmodium* targets.

SIGNIFICANCE

Plasmodium falciparum, the most lethal malaria parasite, has a bleak history of developing resistance to drugs that can become widespread and threaten the success of control measures. Classes of drugs that utilize alternative mechanisms to kill parasites are desperately needed to strengthen the arsenal of weapons against malaria. Our engineered peptide, cPF4PD, has captured the intrinsic antiplasmodial activity of the human defense protein PF4, into a stable minimized structure that is amenable to drug development. Its mechanism of action against *Plasmodium* involves disruption of the intracellular digestive vacuole, without damaging host cells. The differential binding, translocation or lysis of membranes by cPF4PD correlates with the different membrane properties of host versus parasite membranes. This membrane-active mechanism is distinct from the mechanism of current drugs, and the antiplasmodial potency and therapeutic index of cPF4PD are more promising than those of other, non-human derived, defense peptides. These findings provide a strong contribution toward antimalarial drug development strategies and highlight the importance of parasite membranes as therapeutic targets.

ACKNOWLEDGEMENTS

This work was supported by the Australian Research Council (FL15010046 to D.J.C, FT150100398 to STH) and the National Health and Medical Research Council, Australia (APP1084965 to D.J.C. and S.T.H.; and APP1066502 to B.J.M.). A.M.L. is supported by an ARC Discovery Early Career Researcher Award (DE160101035).

AUTHOR CONTRIBUTIONS

Conceptualization, N.L., S.T.H, D.J.C. and B.J.M; Methodology & Validation, N.L., S.T.H. and B.J.M.; Investigation, N.L., A.S.M.D., A.M.L., A.E., P.J.H, A.H.B., O.C., S.T.H. and B.J.M.; Writing – Original draft, N.L., S.T.H., B.J.M.; Writing – Review & Editing, all authors; Visualization, N.L. and B.J.M.; Resources & Funding Acquisition, S.T.H., D.J.C. and B.J.M.

DECLARATION OF INTERESTS

The authors declare no competing interests.

REFERENCES

- Assem, N., Ferreira, D.J., Wolan, D.W., and Dawson, P.E. (2015). Acetone-linked peptides: a convergent approach for peptide macrocyclization and labeling. *Angew. Chem. Int. Ed. Engl.* *54*, 8665-8668.
- Asthana, N., Yadav, S.P., and Ghosh, J.K. (2004). Dissection of antibacterial and toxic activity of melittin: a leucine zipper motif plays a crucial role in determining its hemolytic activity but not antibacterial activity. *J. Biol. Chem.* *279*, 55042-55050.
- Bell, A. (2011). Antimalarial peptides: the long and the short of it. *Curr. Pharm. Des.* *17*, 2719-2731.
- Bhatt, S., Weiss, D.J., Cameron, E., Bisanzio, D., Mappin, B., Dalrymple, U., Battle, K.E., Moyes, C.L., Henry, A., Eckhoff, P.A., *et al.* (2015). The effect of malaria control on *Plasmodium falciparum* in Africa between 2000 and 2015. *Nature* *526*, 207-211.

Blasco, B., Leroy, D., and Fidock, D.A. (2017). Antimalarial drug resistance: linking *Plasmodium falciparum* parasite biology to the clinic. *Nat. Med.* 23, 917-928.

Chan, L.Y., Zhang, V.M., Huang, Y.-h., Waters, N.C., Bansal, P.S., Craik, D.J., and Daly, N.L. (2013). Cyclization of the antimicrobial peptide Gomesin with native chemical ligation: influences on stability and bioactivity. *Chembiochem* 14, 617-624.

Craik, D.J., and Du, J. (2017). Cyclotides as drug design scaffolds. *Curr. Opin. Chem. Biol.* 38, 8-16.

de Koning-Ward, T.F., Gilson, P.R., Boddey, J.A., Rug, M., Smith, B.J., Papenfuss, A.T., Sanders, P.R., Lundie, R.J., Maier, A.G., Cowman, A.F., *et al.* (2009). A newly discovered protein export machine in malaria parasites. *Nature* 459, 945-949.

Eda, S., and Sherman, I.W. (2002). Cytoadherence of malaria-infected red blood cells involves exposure of phosphatidylserine. *Cell Phys Biochem* 12, 373-384.

Engelbrecht, D., and Coetzer, T.L. (2016). *Plasmodium falciparum* exhibits markers of regulated cell death at high population density in vitro. *Parasitol. Int.* 65, 715-727.

Epand, R.M. (2016). *Host Defense Peptides and Their Potential as Therapeutic Agents* (Cham : Springer International Publishing : Imprint: Springer).

Ghosh, J.K., Shaool, D., Guillaud, P., Ciceron, L., Mazier, D., Kustanovich, I., Shai, Y., and Mor, A. (1997). Selective cytotoxicity of dermaseptin S3 toward intraerythrocytic *Plasmodium falciparum* and the underlying molecular basis. *J. Biol. Chem.* 272, 31609-31616.

Greenfield, N.J. (2006). Using circular dichroism spectra to estimate protein secondary structure. *Nat. Protoc.* *1*, 2876-2890.

Haldar, K., Bhattacharjee, S., and Safeukui, I. (2018). Drug resistance in *Plasmodium*. *Nat. Rev. Microbiol.* *16*, 156-170.

Hayward, R., Saliba, K.J., and Kirk, K. (2006). The pH of the digestive vacuole of *Plasmodium falciparum* is not associated with chloroquine resistance. *J. Cell Sci.* *119*, 1016.

Henriques, S.T., Deplazes, E., Lawrence, N., Cheneval, O., Chaousis, S., Inserra, M., Thongyoo, P., King, G.F., Mark, A.E., Vetter, I., *et al.* (2016). Interaction of tarantula venom peptide ProTx-II with lipid membranes is a prerequisite for its inhibition of human voltage-gated sodium channel NaV1.7. *J. Biol. Chem.* *291*, 17049-17065.

Henriques, S.T., Lawrence, N., Chaousis, S., Ravipati, A.S., Cheneval, O., Benfield, A.H., Elliott, A.G., Kavanagh, A.M., Cooper, M.A., Chan, L.Y., *et al.* (2017). Redesigning spider peptide with improved antimicrobial and anticancer properties. *ACS Chem. Biol.* *12*, 2324-2334.

Howes, R.E., Patil, A.P., Piel, F.B., Nyangiri, O.A., Kabaria, C.W., Gething, P.W., Zimmerman, P.A., Barnadas, C., Beall, C.M., Gebremedhin, A., *et al.* (2011). The global distribution of the Duffy blood group. *Nat. Commun.* *2*, 266.

Huang, Y.H., Colgrave, M.L., Clark, R.J., Kotze, A.C., and Craik, D.J. (2010). Lysine-scanning mutagenesis reveals an amendable face of the cyclotide Kalata B1 for the optimization of nematocidal activity. *J. Biol. Chem.* *285*, 10797-10805.

Ji, Y., Majumder, S., Millard, M., Borra, R., Bi, T., Elnagar, A.Y., Neamati, N., Shekhtman, A., and Camarero, J.A. (2013). In vivo activation of the p53 tumor suppressor pathway by an engineered cyclotide. *J. Am. Chem. Soc.* *135*, 11623-11633.

Klonis, N., Tan, O., Jackson, K., Goldberg, D., Klemba, M., and Tilley, L. (2007). Evaluation of pH during cytosomal endocytosis and vacuolar catabolism of haemoglobin in *Plasmodium falciparum*. *Biochem. J.* *407*, 343-354.

Krogstad, D.J., Schlesinger, P.H., and Gluzman, I.Y. (1985). Antimalarials increase vesicle pH in *Plasmodium falciparum*. *J. Cell Biol.* *101*, 2302-2309.

Krugliak, M., Feder, R., Zolotarev, V.Y., Gaidukov, L., Dagan, A., Ginsburg, H., and Mor, A. (2000). Antimalarial activities of dermaseptin S4 derivatives. *Antimicrob. Agents Chemother.* *44*, 2442-2451.

Kuhn, Y., Rohrbach, P., and Lanzer, M. (2007). Quantitative pH measurements in *Plasmodium falciparum*-infected erythrocytes using pHluorin. *Cell. Microbiol.* *9*, 1004-1013.

Love, M.S., Millholland, M.G., Mishra, S., Kulkarni, S., Freeman, K.B., Pan, W., Kavash, R.W., Costanzo, M.J., Jo, H., Daly, T.M., *et al.* (2012). Platelet factor 4 activity against *P. falciparum* and its translation to nonpeptidic mimics as antimalarials. *Cell Host Microbe* *12*, 815-823.

Lubell, Y., Dondorp, A., Guerin, P.J., Drake, T., Meek, S., Ashley, E., Day, N.P., White, N.J., and White, L.J. (2014). Artemisinin resistance--modelling the potential human and economic costs. *Malar. J.* *13*, 452.

McCarthy, J.S., Baker, M., O'Rourke, P., Marquart, L., Griffin, P., Hooft van Huijsduijnen, R., and Mohrle, J.J. (2016). Efficacy of OZ439 (artefenomel) against early *Plasmodium falciparum* blood-stage malaria infection in healthy volunteers. *J. Antimicrob. Chemother.* *71*, 2620-2627.

McMorran, B.J., Marshall, V.M., de Graaf, C., Drysdale, K.E., Shabbar, M., Smyth, G.K., Corbin, J.E., Alexander, W.S., and Foote, S.J. (2009). Platelets kill intraerythrocytic malarial parasites and mediate survival to infection. *Science* *323*, 797-800.

McMorran, B.J., Wieczorski, L., Drysdale, K.E., Chan, J.A., Huang, H.M., Smith, C., Mitiku, C., Beeson, J.G., Burgio, G., and Foote, S.J. (2012). Platelet factor 4 and Duffy antigen required for platelet killing of *Plasmodium falciparum*. *Science* *338*, 1348-1351.

McPhee, J.B., and Hancock, R.E. (2005). Function and therapeutic potential of host defence peptides. *J. Pept. Sci.* *11*, 677-687.

Mikhalyov, I., and Samsonov, A. (2011). Lipid raft detecting in membranes of live erythrocytes. *BBA. Biomembranes* *1808*, 1930-1939.

Murray, C.J., Ortblad, K.F., Guinovart, C., Lim, S.S., Wolock, T.M., Roberts, D.A., Dansereau, E.A., Graetz, N., Barber, R.M., Brown, J.C., *et al.* (2014). Global, regional, and national incidence and mortality for HIV, tuberculosis, and malaria during 1990-2013: a systematic analysis for the Global Burden of Disease Study 2013. *Lancet* *384*, 1005-1070.

Pollaro, L., Raghunathan, S., Morales-Sanfrutos, J., Angelini, A., Kontos, S., and Heinis, C. (2015). Bicyclic Peptides Conjugated to an Albumin-Binding Tag Diffuse Efficiently into Solid Tumors. *Mol. Cancer Ther.* 14, 151-161.

Saliba, K.J., Allen, R.J., Zissis, S., Bray, P.G., Ward, S.A., and Kirk, K. (2003). Acidification of the malaria parasite's digestive vacuole by a H⁺-ATPase and a H⁺-pyrophosphatase. *J. Biol. Chem.* 278, 5605-5612.

Saliba, K.J., and Kirk, K. (1999). pH regulation in the intracellular malaria parasite, *Plasmodium falciparum*. H⁽⁺⁾ extrusion via a V-type H⁽⁺⁾-ATPase. *J. Biol. Chem.* 274, 33213-33219.

Salzer, U., and Prohaska, R. (2001). Stomatin, flotillin-1, and flotillin-2 are major integral proteins of erythrocyte lipid rafts. *Blood* 97, 1141-1143.

Sato, H., and Feix, J.B. (2006). Peptide-membrane interactions and mechanisms of membrane destruction by amphipathic alpha-helical antimicrobial peptides. *Biochim. Biophys. Acta* 1758, 1245-1256.

Schenkel, L.C., and Bakovic, M. (2014). Formation and regulation of mitochondrial membranes. *Int. J. Cell Biol.* 2014, 709828.

Shepherd, N.E., Hoang, H.N., Abbenante, G., and Fairlie, D.P. (2005). Single turn peptide alpha helices with exceptional stability in water. *J. Am. Chem. Soc.* 127, 2974-2983.

Sherman, I.W., Eda, S., and Winograd, E. (2004). Erythrocyte aging and malaria. *Cell. Mol. Biol. (Noisy-le-grand)* 50, 159-169.

Srivastava, K., Cockburn, I.A., Swaim, A., Thompson, L.E., Tripathi, A., Fletcher, C.A., Shirk, E.M., Sun, H., Kowalska, M.A., Fox-Talbot, K., *et al.* (2008). Platelet factor 4 mediates inflammation in experimental cerebral malaria. *Cell Host & Microbe* 4, 179-187.

Srivastava, K., Field, D.J., Aggrey, A., Yamakuchi, M., and Morrell, C.N. (2010). Platelet factor 4 regulation of monocyte KLF4 in experimental cerebral malaria. *PLoS One* 5, e10413.

Stewart, J.C.M. (1980). Colorimetric determination of phospholipids with ammonium ferrocyanate. *Anal. Biochem.* 104, 10-14.

Sulyok, M., Rückle, T., Roth, A., Mürbeth, R.E., Chalon, S., Kerr, N., Samec, S.S., Gobeau, N., Calle, C.L., Ibáñez, J., *et al.* (2017). DSM265 for *Plasmodium falciparum* chemoprophylaxis: a randomised, double blinded, phase 1 trial with controlled human malaria infection. *Lancet Infect. Dis.* 17, 636-644.

Takala-Harrison, S., Jacob, C.G., Arze, C., Cummings, M.P., Silva, J.C., Dondorp, A.M., Fukuda, M.M., Hien, T.T., Mayxay, M., Noedl, H., *et al.* (2015). Independent emergence of artemisinin resistance mutations among *Plasmodium falciparum* in Southeast Asia. *J. Infect. Dis.* 211, 670-679.

Tawk, L., Chicanne, G., Dubremetz, J.F., Richard, V., Payrastre, B., Vial, H.J., Roy, C., and Wengelnik, K. (2010). Phosphatidylinositol 3-phosphate, an essential lipid in

Plasmodium, localizes to the food vacuole membrane and the apicoplast. *Eukaryot. Cell* 9, 1519-1530.

Totino, P.R.R., Magalhães, A.D., Silva, L.A., Banic, D.M., Daniel-Ribeiro, C.T., and Ferreira-da-Cruz, M.d.F. (2010). Apoptosis of non-parasitized red blood cells in malaria: a putative mechanism involved in the pathogenesis of anaemia. *Malar. J.* 9, 350.

Trape, J.F., Tall, A., Diagne, N., Ndiath, O., Ly, A.B., Faye, J., Dieye-Ba, F., Roucher, C., Bouganali, C., Badiane, A., *et al.* (2011). Malaria morbidity and pyrethroid resistance after the introduction of insecticide-treated bednets and artemisinin-based combination therapies: a longitudinal study. *Lancet Infect. Dis.* 11, 925-932.

Troeira Henriques, S., Lawrence, N., Chaousis, S., Ravipati, A.S., Cheneval, O., Benfield, A.H., Elliott, A.G., Kavanagh, A.M., Cooper, M.A., Chan, L.Y., *et al.* (2017). Redesigned spider peptide with improved antimicrobial and anticancer properties. *ACS Chem. Biol.* 12, 2324-2334.

Vale, N., Aguiar, L., and Gomes, P. (2014). Antimicrobial peptides: a new class of antimalarial drugs? *Front. Pharmacol.* 5, 275.

Vranken, W.F., Boucher, W., Stevens, T.J., Fogh, R.H., Pajon, A., Llinas, P., Ulrich, E.L., Markley, J.L., Ionides, J., and Laue, E.D. (2005). The CCPN data model for NMR spectroscopy: Development of a software pipeline. *Proteins Struct. Funct. Bioinform.* 59, 687-696.

Wells, T.N.C., van Huijsduijnen, R.H., and Van Voorhis, W.C. (2015). Malaria medicines: a glass half full? *Nat. Rev. Drug Discov.* 14, 424-442.

White, N.J., Duong, T.T., Uthaisin, C., Nosten, F., Phyo, A.P., Hanboonkunupakarn, B., Pukrittayakamee, S., Jittamala, P., Chuthasmit, K., Cheung, M.S., *et al.* (2016).

Antimalarial activity of KAF156 in *Falciparum* and *Vivax* malaria. *N. Engl. J. Med.* 375, 1152-1160.

White, N.J., Pukrittayakamee, S., Phyo, A.P., Rueangweerayut, R., Nosten, F., Jittamala, P., Jeeyapant, A., Jain, J.P., Lefèvre, G., Li, R., *et al.* (2014). Spiroindolone KAE609 for *Falciparum* and *Vivax* malaria. *N. Engl. J. Med.* 371, 403-410.

WHO (2016). World Malaria Report 2016. World Health Organisation.

Wishart, D.S., Bigam, C.G., Holm, A., Hodges, R.S., and Sykes, B.D. (1995). H-1, C-13 and N-15 random coil Nmr chemical-shifts of the common amino-acids .1. Investigations of nearest-neighbor effects (Vol 5, Pg 67, 1995). *J. Biomol. NMR* 5, 332-332.

Yeaman, M.R., and Yount, N.Y. (2003). Mechanisms of antimicrobial peptide action and resistance. *Pharmacol. Rev.* 55, 27-55.

Yeaman, M.R., Yount, N.Y., Waring, A.J., Gank, K.D., Kupferwasser, D., Wiese, R., Bayer, A.S., and Welch, W.H. (2007). Modular determinants of antimicrobial activity in platelet factor-4 family kinocidins. *Biochim. Biophys. Acta* 1768, 609-619.

Zucker, M.B., and Katz, I.R. (1991). Platelet Factor-IV - production, structure, and physiological and immunological action. *Proc. Soc. Exp. Biol. Med.* 198, 693-702.

MAIN FIGURE TITLES AND LEGENDS

Figure 1. Antiplasmodial activity of PF4 peptide domains. **A.** Primary amino acid sequence of recombinant human PF4 – indicating the location of chemokine (orange) and antiplasmodial (bold) domains – and showing the location of PF4-derived peptides included in this study. See also Table S1; **B.** PF4 cartoon (PDB:1F9Q) showing the arrangement of C-terminal α -helices (antiplasmodial) as head-to-tail dimers (black box) and chemokine domains (orange circles); **C.** Inhibition of *P. falciparum* growth in human RBCs treated with increasing concentrations of recombinant full length PF4 or C-terminal peptide PF4P₃₅₋₇₀, as determined by flow cytometry analysis. Data points are mean \pm SD from \geq two independent replicates; **D.** Inhibition of *P. falciparum* growth in human RBCs from donors with the Duffy antigen receptor for chemokines (DARC) present +/+ (Donor A) or absent -/- (Donors B, C, D) for the truncated PF4₃₅₋₇₀ compared to full length PF4. Individual data points are shown from two independent replicates, bars represent averages.

Figure 2. Structure and stability of minimized PF4 peptides. **A.** Cartoon showing the predicted structure of the C-terminal PF4 peptide (PF4P₅₇₋₇₀), where charged Lys residues (K5, K6, K9, K10) are present on one side of an α -helix. Tyr (Y4, orange), Ile and Leu (not shown) are present on the opposite side, where they contribute to hydrophobic interactions between the helices in the peptide dimers – open PF4 peptide dimer (PF4PD) and closed cyclic PF4 peptide dimer (cPF4PD); **B.** Circular dichroism (CD) spectra of the peptides, where the presence of α -helical structure is indicated by mean residual ellipticity (θ) minima at 208 and 222 nm. Spectra for peptides in aqueous

solution (100 mM NaF, 10 mM KH₂PO₄ pH 7.5) are shown in blue, and 1:1 aqueous solution with helix inducing trifluoroethanolamine (TFE) are shown in grey; **C.** 2D NMR secondary α H shifts for peptides in aqueous solution (10% D₂O/90% H₂O v/v), where α -helical structure is indicated for residues with secondary alpha proton shifts ≤ -0.1 (blue boxes). Symbols (#,*,^) denote ambiguity of α H shifts between these residues due to peak overlap. See also Table S2; **D.** Peptide stability following up to 24 h incubation in human serum (25% v/v) as a percentage of peptide recovered at 0 h. Values have been calculated from area under the curve for recovered peptide peaks at 215 nm using analytical RP-HPLC. Data points are mean \pm SD from three replicates.

Figure 3. Antiplasmodial activity of minimized PF4 peptides and selective entry into *Plasmodium*-infected RBCs. **A.** Inhibition of *P. falciparum* growth in human RBCs treated with increasing concentrations of minimized PF4 peptides. Data points are mean \pm SD from three independent replicates; **B.** Hemolysis of RBCs (0.25% v/v) collected from healthy human donors following incubation with increasing concentrations of peptides. Melittin was included as a control for membrane lysis (Asthana et al., 2004). Data points are mean \pm SD from three biological replicates; **C.** Internalization of increasing concentrations of cPF4PD-A488 into RBCs, comparing uninfected RBCs (uRBC) and RBCs infected with ring and trophozoite stage *P. falciparum* (iRBC). Data points are mean \pm SD from two independent replicates; **D.** Fluorescence micrographs showing uninfected RBCs, and ring and trophozoite stage infected RBCs treated with 20 μ M cPF4PD-A488; **E.** Fluorescence micrographs showing uninfected and trophozoite stage infected RBCs that were either untreated or treated with 20 μ M

cPF4PD-A488. Selective staining shows: DAPI, DNA location; Exp2, location of intact parasite parasitophorous vacuole membrane (PVM); A488, intracellular localization of cPF4PD-A488. All experiments were conducted in DARC-positive RBCs. The scale bars represent 5 μm .

Figure 4. Mechanism of action of cPF4PD inside RBCs infected with *P.*

***falciparum*. A.** Micrographs showing Plasmepsin II-GFP transgenic *P. falciparum*-infected RBCs untreated and treated with 20 μM cPF4PD, with selective staining: DAPI shows DNA location, TUNEL shows DNA fragmentation indicating parasite death, GFP shows location of parasite DV protein Plasmepsin II. The scale bars represent 5 μm ; **B.** Proportion of infected RBCs with GFP expanded location indicating DV lysis, and \pm TUNEL staining indicating parasite death from 1.5 to 9 h following treatment with 20 μM cPF4PD, compared to untreated infected RBCs. Bars represent mean \pm SD from two independent replicates; **C.** Left panel: Representative fluorescence traces showing alkalinization of the DV in saponin-isolated trophozoite-stage *P. falciparum* immediately following treatment with cPF4PD or the V-type H^+ pump inhibitor conanamycin A (Con A, positive control). An increase in fluorescence ratio corresponds to an increase in pH_{DV} . For the purpose of this study the relationship between the fluorescence ratio and pH_{DV} was not calibrated. Right panel: Concentration-dependent effect of cPF4PD on the initial rate of DV alkalinization (calculated from a linear regression of the fluorescence ratio data obtained in the first 1000 s). Data points are mean \pm SD from three biological replicates; **D.** Fluorescence trace showing the effects of cPF4PD and Con A on cytosolic pH (pH_i) in saponin-isolated trophozoite-stage *P. falciparum*. The data are from

a single experiment and are representative of those obtained in three similar experiments.

Figure 5. Selective phospholipid binding and membrane penetration of minimized

PF4 peptides. A. Peptide lipid association curves for POPC (PC, dashed line) and POPC/POPS (PC/PS 4:1, solid line) lipid bilayers. P/L_{\max} was determined at the end of the association phase ($t = 170$ s) for each peptide concentration injected over lipid bilayers on an L1 chip; **B.** SPR sensorgrams obtained with peptide samples ($16 \mu\text{M}$) injected over POPC/POPS (PC/PS 4:1) lipid bilayers **C.** cPF4PD peptide lipid association curves for neutral (POPC (PC), PC/Chol/SM 2.7:3.3:4), and anionic (POPC/POPS (PC/PS 4:1, 3:2), POPC/POPG (PC/PG 4:1), POPC/PI (PC/PI 4:1)) phospholipid bilayers. P/L_{\max} was determined as above; **D.** Peptide-induced leakage of CF-loaded phospholipid vesicles was determined by measuring CF dequenching ($\lambda_{\text{exc}}=485 \text{ nm}/ \lambda_{\text{em}}=520 \text{ nm}$) following incubation with increasing concentrations of peptide. Peptide concentrations required to permeabilize 50% of $5 \mu\text{M}$ vesicles (PC_{50}) values determined from the vesicle leakage curves for POPC/POPS (PC/PS) vs POPC (PC) were: PF4P, $1.50 \pm 0.07 \mu\text{M}$ and $>10\mu\text{M}$; PF4PD, $0.020 \pm 0.002 \mu\text{M}$ and $>2.5\mu\text{M}$; cPF4PD, $0.058 \pm 0.008 \mu\text{M}$ and $>10\mu\text{M}$. Data points are mean \pm SD from three independent replicates.

STAR METHODS

CONTACT FOR REAGENT AND RESOURCE SHARING

Further information and requests for resources and reagents should be directed to and will be fulfilled by the Lead Contact, Brendan McMorran (brendan.mcmorran@anu.edu.au).

EXPERIMENTAL MODEL AND SUBJECT DETAILS

Plasmodium falciparum culture

P. falciparum was cultured in O⁺ human RBC and cell culture medium (CCM) comprising RPMI 1640 supplemented with 8.8 mM D-glucose, 22 mM HEPES, 208 nM hypoxanthine (Sigma-Aldrich, Missouri, US), 46.1 nM gentamicin, 2.1 g/L AlbuMAX® I, 2.8 mM L-glutamine (ThermoFisher Scientific, Australia), and 4.2% (v/v) O⁺ human serum. Cultures were maintained in flasks filled with 1% O₂/3% CO₂/96% N₂ gas mix, and kept in an orbital shaking incubator at 50 rpm at 37°C. Culture parasitemia was maintained between 0.5% and 10%, and CCM was changed every 1-2 days. The RBC and sera were from anonymous adult blood donors, aged 18-60 years, provided by the Australian Red Cross Blood Service.

For the cytosolic and digestive vacuole pH assays, *P. falciparum* parasites (3D7 strain) were maintained in serum-free CCM (RPMI 1640 containing 25 mM HEPES and supplemented with 3 g/L Albumax II, 11 mM additional glucose, 200 µM hypoxanthine and 20 µg/mL gentamicin sulfate).

Human red blood cells from healthy donors

Whole blood was collected from finger prick (~100 µl total) from two females and one male donor (adult donors, aged 25-50 years, blood type not recorded), and RBCs were prepared and used as separate biological replicates.

Ethics statement

Experimental procedures involving human blood were approved by The Australian National University Human Research Ethics Committee, approval numbers 2014/765, 2011/266 and 2017/351; and The University of Queensland approval number 2013000582.

METHOD DETAILS

Purchased PF4 and peptides

Recombinant human PF4 (>98% purity by SDS-PAGE and HPLC) was purchased from Peptotech, NJ (USA). PF4P₁₋₃₅ and PF4P₃₆₋₇₀ (>98% purity by HPLC and MS) were purchased from Mimotopes, Vic (Aus).

Synthesized peptides

PF4P₅₇₋₇₀, PF4PD and cPF4PD were synthesized on rink amide resin using automated synthesis (Symphony, Protein Technologies Inc) by standard Fmoc solid-phase chemistry. Peptides were deprotected and cleaved from the resin using H₂O:triisopropylsilane:trifluoroacetic acid (TFA) (2:2:96, v/v/v) for 2.5 h at room temperature. The resin was filtered and the TFA evaporated under vacuum. All crude deprotected linear peptides were then precipitated with ice-cold diethyl ether and extracted with 50% acetonitrile (ACN): 0.05% TFA. All peptides were purified by RP-

HPLC using Shimadzu preparative system and Phenomenex Jupiter C18 column with a 1%/min gradient of solvent B (90% ACN, 0.05% TFA v/v) against solvent A (0.05% v/v TFA) and a flow rate of 8 mL/min. cPF4PD was then dissolved in 50% ACN, 0.05% TFA (v/v) at 0.5 mg/mL, flushed for 5 minutes with nitrogen and oxidized in 50% ACN, 20 molar equivalents of iodine solution for 30 min at room temperature, in the dark. The oxidizing buffer was then quenched with ascorbic acid, diluted by half with water and purified by RP-HPLC as above. The mass of the peptides was confirmed by ESI-MS (Figure S1 panel A, Table S1). Purity >95% of the peptides was confirmed by RP-HPLC with a 2%/min gradient of solvent A (0.1% formic acid) to solvent B (90% ACN, 0.1% formic acid, see Figure S1 panel B). Peptide sample concentration was determined by absorbance at 280 nm (see Table S1). Overall hydrophobicity of the peptides was compared by RP-HPLC with a 1%/min gradient of solvent A (0.1% TFA) to solvent B (90% ACN, 0.1% TFA, see Table S1).

Preparation of cPF4PD-A488

Labeling of cPF4PD with A488 was performed using oxime ligation (Assem et al., 2015) to produce a labeled peptide with a single A488 probe between Cys 2 and Cys 33 (see Figure S3, Panel A). Peptide (5 mg) was reacted with 1.1 molar equivalents of tris-(2-carboxyethyl) phosphine (TCEP) and 1.5 molar equivalents of dichloroacetone in 30 mL of NH_4HCO_3 pH 8.1 for 2 h at room temperature, to produce a macrocyclic ketone. The peptide was purified by RP-HPLC as above. To selectively add the label onto the acetone linker, 0.5 mg of the purified macrocyclic ketone peptide was reacted with 2 molar equivalents of Alexafluor 488 hydroxylamine dye (ThermoFischer Scientific) in

200 μ l of 50 mM NaOAc, 150 mM NaCl pH 5 at 37°C overnight. The labeled peptide was purified by RP-HPLC and the correct mass confirmed by ESI-MS (Figure S3, panel B and Table S1). Cyclization of the PF4P dimer peptide with an acetone linker (labeled peptide) compared to a disulfide bond (unlabeled peptide), and addition of the A488 label did not affect the peptide's biological activity. Relative biological activity compared to unlabeled cPF4PD, was estimated by binding to a POPC/POPS (4:1) model lipid bilayer using SPR (Figure S3, panel C).

Circular dichroism spectroscopy

Overall secondary structure was estimated using CD spectroscopy (Greenfield, 2006). Peptides were prepared at 50 μ M in aqueous solution (100 mM NaF, 10 mM KH_2PO_4 pH 7.5) or a 1:1 mixture of aqueous solution with helix inducing trifluoroethanolamine (TFE). NaF was included in the aqueous solution to provide Na^+ ions. F^- ions produce superior spectra below 200 nm compared to Cl^- ions, hence the avoidance of NaCl (Greenfield, 2006). CD spectra were collected and averaged from 5 scans, at 1 nm intervals between wavelengths of 185 nm to 260 nm, using a Jasco J810 spectropolarimeter. Blanks were subtracted, and the mean residual ellipticity (θ) was calculated using the formula: $\theta = mdeg / (c \cdot l \cdot N_{res})$, where *mdeg* is the CD output in millidegrees, *c* is the molar peptide concentration, *l* is the light path length in mm and N_{res} is the number of amino acid residues. The percentage of helical conformation was calculated using the formula: $H_a = (\theta_{222nm} - \theta_C) / (\theta^{\infty 222nm} - \theta_C)$, with θ_{222nm} the lowest value between 218 and 222nm, $\theta_C = 2220 - 53T$ and $\theta^{\infty 222nm} = (-44000 + 250T)(1 - k / N_{res})$ with T in °C and k=3.0 (Shepherd et al., 2005).

NMR spectroscopy

Samples of PF4PD and cPF4PD were prepared by dissolving peptide in 10% D₂O/90% H₂O (v/v) at a concentration of ~1 mM and pH of 3.5. Spectra were recorded on a Bruker Avance III 600 MHz NMR spectrometer at 298K, and using excitation sculpting as solvent suppression. Chemical shifts of backbone resonances were assigned by analysis of 2D TOCSY (with an 80 ms MLEV-17 spin lock) and NOESY (mixing time of 200 ms). See Figure S2. Spectra were processed with Topspin 3.5 (Bruker Biospin) and analysed with CcpNMR analysis (Vranken et al., 2005). Secondary α H chemical shifts were calculated as the difference between the observed α H chemical shifts and that of the corresponding residues in a random coil peptide (Wishart et al., 1995).

Peptide stability in human serum

The stability of peptides in human serum was determined by quantifying the amount of intact peptide remaining using analytical RP-HPLC (Chan et al., 2013). Peptides were added to a solution of 25% (v/v) serum in phosphate buffered saline (PBS; 137 mM NaCl, 2.7 mM KCl, 10 mM Na₂HPO₄, 1.8 mM KH₂PO₄) at a final concentration of 50 μ M. Controls with peptide in PBS were also included. Peptides with serum or PBS were incubated at 37°C, and samples were removed from the serum after incubation for 0, 2, 4, 8 and 24 h, and the PBS incubations at 0 and 24 h. The enzymatic reaction was stopped by adding 2x volume of ACN with 2% (v/v) TFA and incubating on ice for 10 min. The peptide was recovered by centrifuging at 4°C for 20 min, then collecting the supernatant. The supernatant containing peptide was added to 2x volume of HPLC

solvent A. The diluted sample was analyzed using RP-HPLC (1%/min gradient of solvent B, as above), and the area under the curve at 215 nm was measured for the peak corresponding to full-length peptide (as confirmed by ESI-MS). The amount of peptide remaining was calculated as a percentage of the amount of peptide recovered following 0 h incubation with 25% (v/v) serum. No appreciable peptide degradation was detected for the peptides in PBS over 24 h.

RBC hemolysis assays

Peptides were tested for hemolytic activity against RBCs collected from healthy human volunteers (adults aged 25-50 years) (Huang et al., 2010). Blood drops from a finger prick were dropped into phosphate buffered saline (PBS) in a 1.5 mL tube. RBCs were harvested by centrifugation at 4000 rpm for 1 min. The supernatant was removed and the RBCs were washed 3 times by resuspending in PBS followed by centrifugation as before. A solution of 0.5% RBCs in PBS (v/v) was prepared and added to 96-well plates (50 μ l), and an equal volume of serially diluted peptide in PBS was added to the cells. Triton X-100 (0.1% v/v final) was included as a control to measure 100% hemolysis, and PBS to measure 0% hemolysis. Melittin peptide was also included as a control for membrane lysis (Asthana et al., 2004). Plates were centrifuged 1000 rpm for 5 min to pellet RBCs. The supernatant was transferred to a flat bottom 96-well plate and the absorbance at 415 nm was recorded to detect released hemoglobin. The percentage hemolysis was calculated using the following formula: $(A_{415} \text{ sample} - A_{415} \text{ PBS}) / (A_{415} \text{ TX-100} - A_{415} \text{ PBS}) \times 100$.

Peptide treatment

Peptide treatments of parasites to measure parasite growth, uptake of cPF4PD-A488, and for the immunofluorescence studies were conducted using peptides diluted in CCM and added to parasites (0.5% parasitemia) that were synchronized at the ring stage the day before experiments using 5% (w/v) D-sorbitol incubation for 10 minutes. All parasite experiments used Duffy antigen receptor for chemokine (DARC) positive RBCs from adult donors (aged 18-60 years), unless stated otherwise. Parasites were incubated with peptides at 37°C for 48 h (growth assays), 1 h (cPF4PD-A488 treatment) or between 1 and 9 h (immunofluorescence studies), and then washed in PBS and fixed in 1% (w/v) formaldehyde (Cytotfix™ diluted ¼ with PBS, BD Biosciences, Australia) for at least 24 h at 4°C. Fixed cells were washed with PBS containing 1% (w/v) bovine serum albumin (PBS-BSA) and stained with 5 µg/mL Hoechst 33342 (Life Technologies, Australia) for 5 min at 4°C. Fluorescence signals were measured using LSR Fortessa cell analyzer (BD Biosciences); at least 100,000 events were collected per sample. Percentages of infected cells and mean fluorescence intensity of cPF4PD-A488 treated parasites were identified and enumerated using FACSDiva software (BD Biosciences). Percentage parasite growth was determined using the formula:

% Parasite growth = (treatment parasitemia - initial parasitemia) / (no treatment parasitemia - initial parasitemia) x 100.

Immunofluorescence and TUNEL labelling

Immunofluorescence and deoxyuridine triphosphate nick-end labelling by the terminal deoxynucleotidyl transferase (TUNEL) labelling, which labels degraded or sheared DNA

and reveals parasite apoptosis or necrosis, were performed on fixed parasite culture samples. Cells were washed and diluted into PBS, smeared onto glass slides coated with polyethylenimine (0.1% v/v), air dried (5 min), and additionally fixed using 25% Cytotfix/Cytoperm (BD Biosciences) solution diluted in PBS. Cell smears were incubated overnight at 4°C with primary antibodies diluted in PBS containing PBS-BSA, rabbit polyclonal anti-*Pf*Exp2 (gift from P. Gilson, Burnet Institute, Australia) to label the parasite parasitophorous vacuole (de Koning-Ward et al., 2009), or polyclonal chicken anti-GFP (Abcam, Australia) to label GFP-tagged plasmepsin II, which is expressed exclusively in the parasite digestive vacuole (Klonis et al., 2007). After washing in PBS containing 1% BSA, cells were incubated at room temperature for 1 h with secondary antibodies, anti-rabbit Alexa Fluor650 or anti-chicken Alexa Fluor488 conjugates (ThermoFisher Scientific), prepared in PBS containing PBS-BSA. TUNEL staining used the Apo BrdU TUNEL Assay Kit (ThermoFisher Scientific), and TUNEL-labelled DNA was detected using a biotinylated anti-BrdU antibody and streptavidin-Alexa Fluor 594 conjugate (ThermoFisher Scientific). After labelling and staining, slides were washed in PBS and mounted in SlowFade™ Gold Antifade Mountant with DAPI (ThermoFisher Scientific, Australia) and glass coverslips (#1 from Menzel-Gläser). Slides were examined at room temperature using an Axio Observer inverted fluorescence microscope using 630× magnification and coupled to a AxioCam 503 monochrome camera (Zeiss, Australia). All images were acquired and processed using Zen microscope and imaging software (Zeiss, Australia). At least 100 infected cells were counted on each slide, and each time point was assayed in duplicate.

Parasite digestive vacuole pH

Parasite digestive vacuole pH (pH_{DV}) was monitored in parasites containing the membrane-impermeant fluorescent pH indicator fluorescein-dextran (10,000 MW; Molecular Probes, Thermo Fisher Scientific) in their DVs (Krogstad et al., 1985; Saliba et al., 2003). First, uninfected RBCs were loaded with fluorescein-dextran by lysing then resealing them in the presence of the dye. Lysis solution (5 mM HEPES, 11 mM glucose, 2 mM MgCl_2 and 2 mM ATP; pH 7.4; 2.25 mL) containing 55 μM of the fluorophore was added to packed RBCs (1 mL), and the resulting mixture was incubated at 30°C for 10 min. RBCs were then resealed by the addition of 2.25 mL of a pre-warmed (37°C), pH 7.4 solution containing 280 mM NaCl, 40 mM KCl, 11 mM glucose and 1 mM HEPES. The dye-loaded RBCs were washed three times (1200 $\times g$, 5 min) in RPMI 1640 medium (containing 25 mM HEPES and supplemented with 11 mM additional glucose, 200 μM hypoxanthine and 20 $\mu\text{g}/\text{mL}$ gentamicin sulfate), and either used immediately or stored (as packed erythrocytes protected from light) at 4°C for up to two weeks. Dye-loaded RBCs were inoculated with trophozoite-infected RBCs that were separated from uninfected RBCs using a VarioMACS magnet and CS column. Experiments were performed approximately 48 h later, after which time daughter parasites had invaded dye-loaded erythrocytes and endocytosed the dye-containing erythrocyte cytosol into their DVs as they matured into trophozoites. The trophozoites were functionally isolated from their host RBCs by brief exposure of the cell suspensions to saponin (0.05% w/v, of which $\geq 10\%$ was the active agent sapogenin). The parasites were sedimented by centrifugation (1000 $\times g$, 5 min) then washed several times (12,000 $\times g$, 30 s) in 'Saline Solution' (125 mM NaCl, 5 mM KCl, 1 mM MgCl_2 , 20

mM glucose and 25 mM HEPES; pH 7.1). Fluorescence measurements were performed using a Tecan fluorescence spectrometer plate-reader, with parasites suspended at 37°C at a density of $1-2 \times 10^7$ cells/mL in Saline Solution. The suspensions were excited at 440 and 495 nm successively and emission was recorded at 520 nm. The ratio of the two measurements (495 nm/440 nm) was used as an indicator of pH_{DV}.

Parasite cytosolic pH

Mature trophozoite-stage 3D7 *P. falciparum* parasites were functionally isolated from their host erythrocytes as described above then washed several times in 'Bicarbonate-free Medium' (bicarbonate-free RPMI 1640 supplemented with 25 mM HEPES, 11 mM additional glucose and 0.2 mM hypoxanthine; pH 7.1). Parasites were loaded with the ratiometric pH-sensitive dye 2',7'-Bis-(2-Carboxyethyl)-5-(and-6)-Carboxyfluorescein, (BCECF) by incubating parasites with the acetoxymethyl ester form of the dye (1 μ M BCECF-AM; Molecular Probes, Thermo Fisher Scientific) at 37°C for 10 min (Saliba and Kirk, 1999). The parasites were then washed several times in Bicarbonate-free Medium ($12,000 \times g$, 30 s) to remove the remaining extracellular dye. For measurements of pH, parasites were suspended at 37°C at a density of $1-2 \times 10^7$ cells/mL in Saline Solution. The suspensions were excited at 440 nm and 495 nm successively using a PerkinElmer LS 50B fluorescence spectrometer with a dual excitation Fast Filter accessory, with emission recorded at 520 nm. The ratio of the two measurements (495 nm/440 nm) provides a measure of cytosolic pH. The relationship between the fluorescence ratio and cytosolic pH was calibrated by suspending parasites in calibration saline solutions

(130 mM KCl, 1 mM MgCl₂, 20 mM glucose, 25 mM HEPES) adjusted to different pH values and adding the K⁺/H⁺ ionophore nigericin (30 μM) (Saliba and Kirk, 1999).

Liposome preparation

Synthetic lipids (POPC, POPS, POPG, PI and SM) were purchased from Auspep (Australian distributor of Avanti Polar Lipids). Synthetic cholesterol (Chol) was purchased from Sigma. The required lipid mixtures were prepared in chloroform, and a lipid film was then prepared by drying under nitrogen, then in a vacuum desiccator for >2 h. Lipid vesicles of 50 nm (small unilamellar vesicles, SUV) or 100 nm (large unilamellar vesicles, LUV) diameter were prepared using repeated freeze/thaw cycles followed by extrusion of 1 mM lipid mixtures in HEPES buffer (10 mM HEPES, 150 mM NaCl, pH 7.4) (Troeira Henriques et al., 2017).

Binding of peptides to lipid bilayers

Peptide-membrane interactions were followed by SPR at 25°C with an L1 biosensor chip in a Biacore 3000 instrument (GE healthcare). SUVs composed of POPC, POPC/POPS (4:1 molar ratio), POPC/POPS (3:2), POPC/POPG (4:1), POPC/PI (4:1) and POPC/Chol/SM (27:33:40) were prepared in HEPES buffer and deposited onto an L1 chip for 40 min at a flow rate of 2 μl/min, reaching a steady-state plateau and confirming chip surface coverage of deposited lipid bilayers (Henriques et al., 2016) Serial dilutions of peptides were prepared in HEPES buffer and injected over the lipid bilayer (flow rate 5 μl/min, 180 s). Peptide-lipid dissociation was followed

for 600 s. Response units (RU) from sensorgrams were converted to peptide to lipid ratio (P/L, mol/mol), assuming $1 \text{ RU} = 1 \text{ pg/mm}^2$ lipid or peptide. The maximum P/L (mol/mol) achieved at the end of the association phase (170s) was calculated to normalize the response to the molecular weight of each peptide and the deposition level achieved for each lipid system to allow comparison of binding between peptides and across different lipid mixtures.

Vesicle leakage assay

Membrane leakage of POPC and POPC/POPS (4:1) LUVs were prepared as above, except with 50 mM CF in HEPES buffer. CF-loaded vesicles were purified using a 10 mL gel filtration column prepared from pre-swollen Sephadex G-50 beads in HEPES buffer. The lipid concentration of the purified vesicles was determined against a standard curve prepared with Ferrothiocyanate Reagent (100 mM $\text{FeCl}_3 \cdot 6\text{H}_2\text{O}$, 400 mM NH_4SCN ; Stewart assay (Stewart, 1980)). Serial dilutions of peptide (prepared in HEPES buffer) were incubated with LUVs containing 5 μM lipid in black 96-well plates. The fluorescence intensity (FI; excitation at 489nm, emission at 515nm) was measured using a Tecan fluorescence spectrometer plate-reader after a 10 min incubation. In preliminary studies the fluorescence emission intensity was measured after 5 and 15 min incubations and no differences in the leakage efficiency were detected. Triton X-100 (0.1% v/v) was included to measure 100% leakage, and HEPES buffer to measure 0% leakage. The percentage of leakage induced by the peptides was calculated using the formula: $(FI \text{ sample} - FI \text{ HEPES}) / (FI \text{ TX-100} - FI \text{ HEPES}) \times 100$.

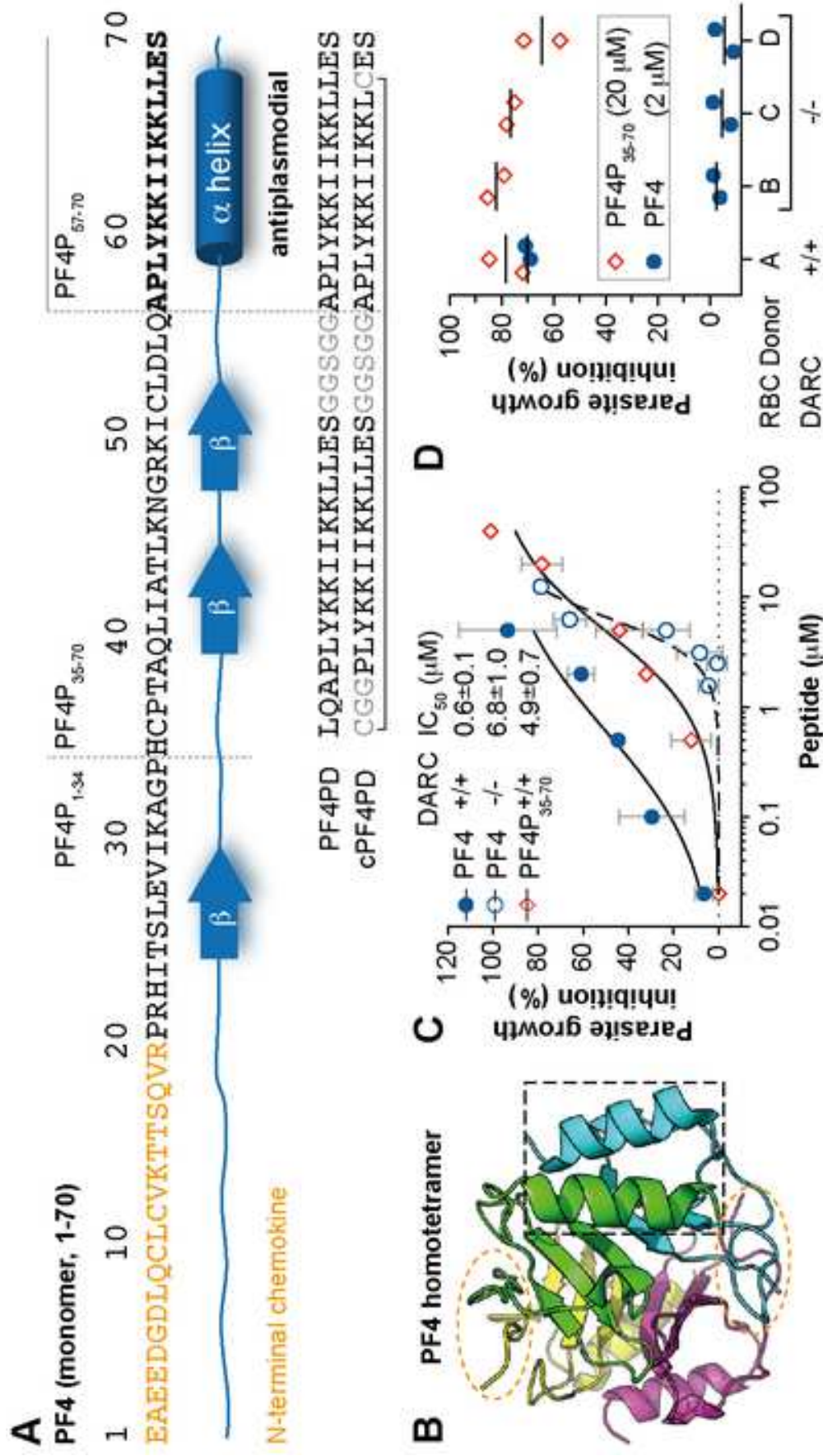
QUANTIFICATION AND STATISTICAL ANALYSIS

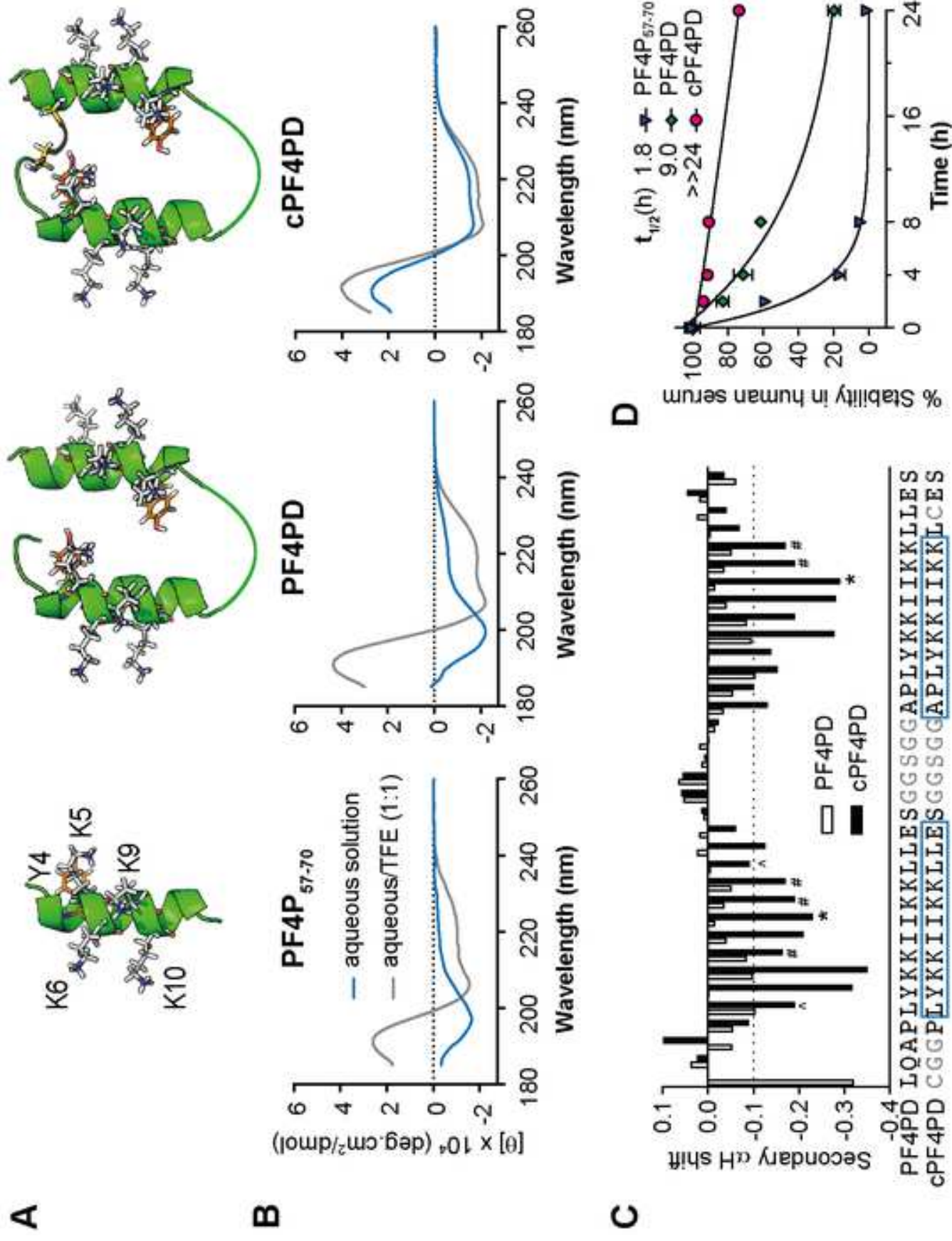
Data collection

Data presented herein was replicated in separate experiments, performed on different days (n). Unless otherwise stated, data points shown in figures are the mean of independent data, and the error represents standard deviation (SD).

Non-linear regression for data analysis

Prism 7.0 (GraphPad Software, Inc) was used to fit all non-linear regression curves as follows: dose response curves – One site Specific binding with Hill slope, and constraining Bmax to 100%; serum stability – One phase decay; Peptide/lipid binding curves – One site Specific binding.





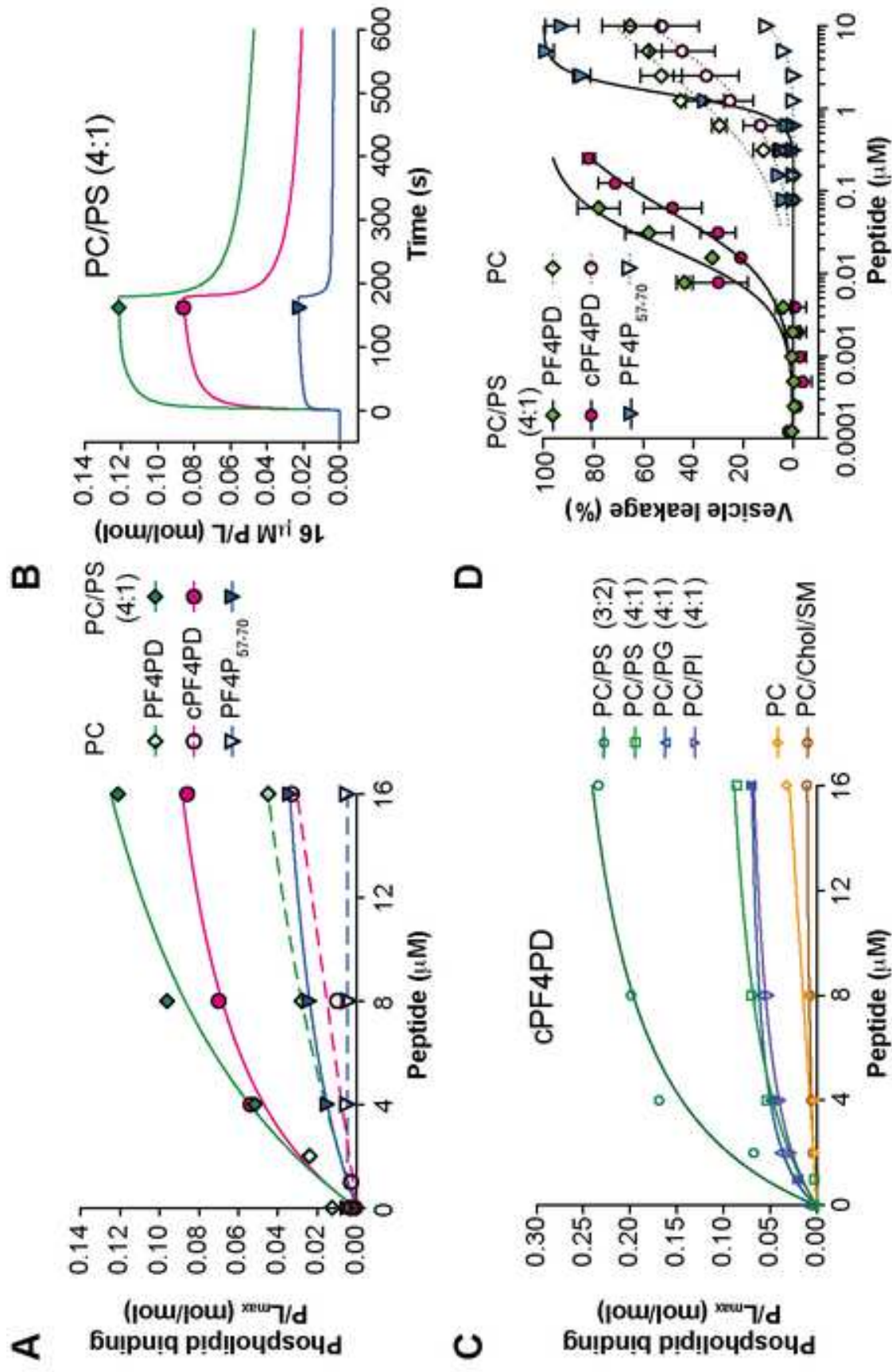


Figure 3

[Click here to download Figure Figure 3_s.tif](#)

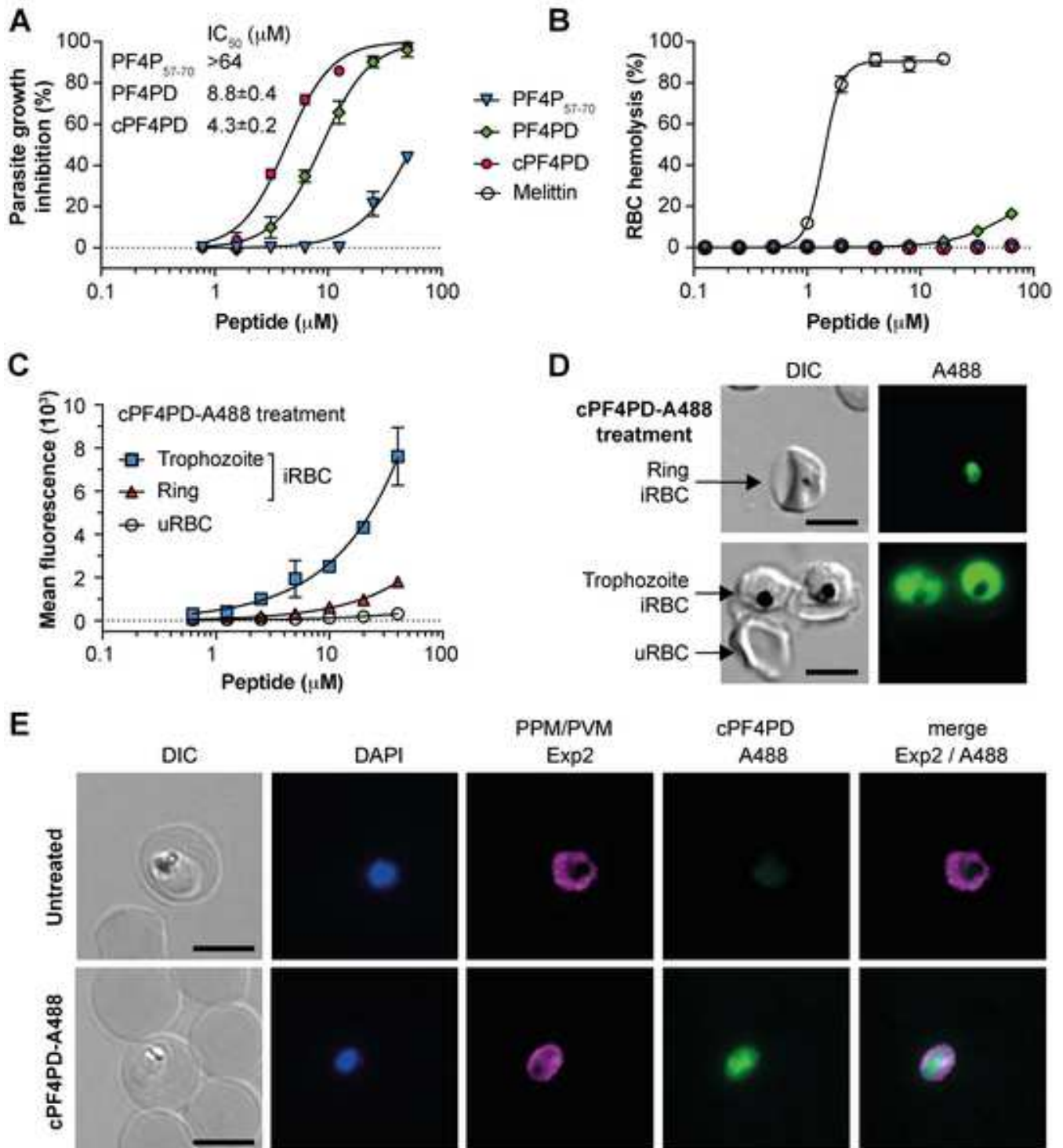
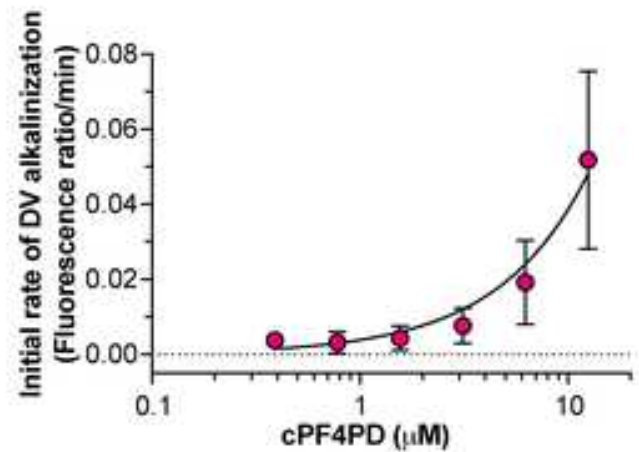
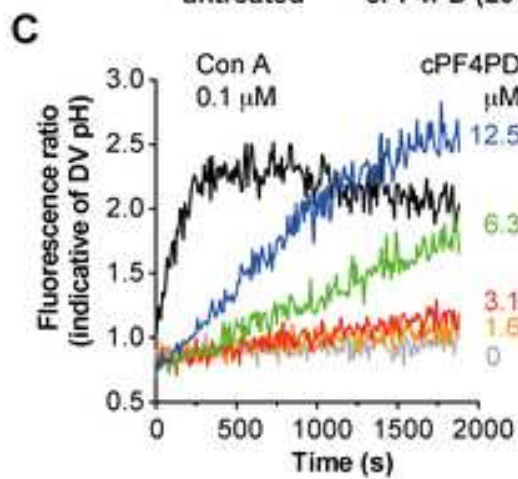
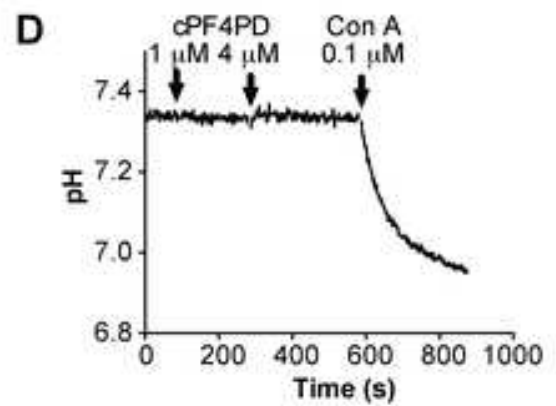
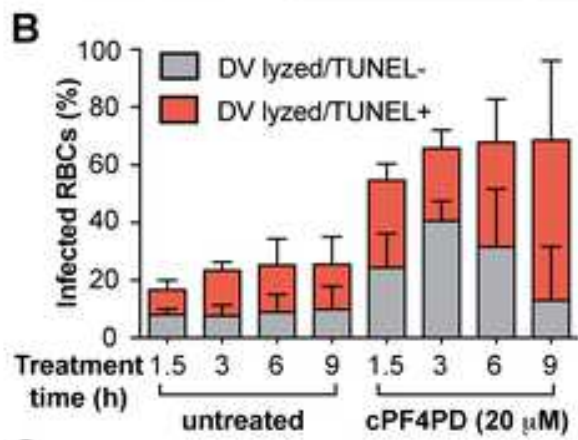
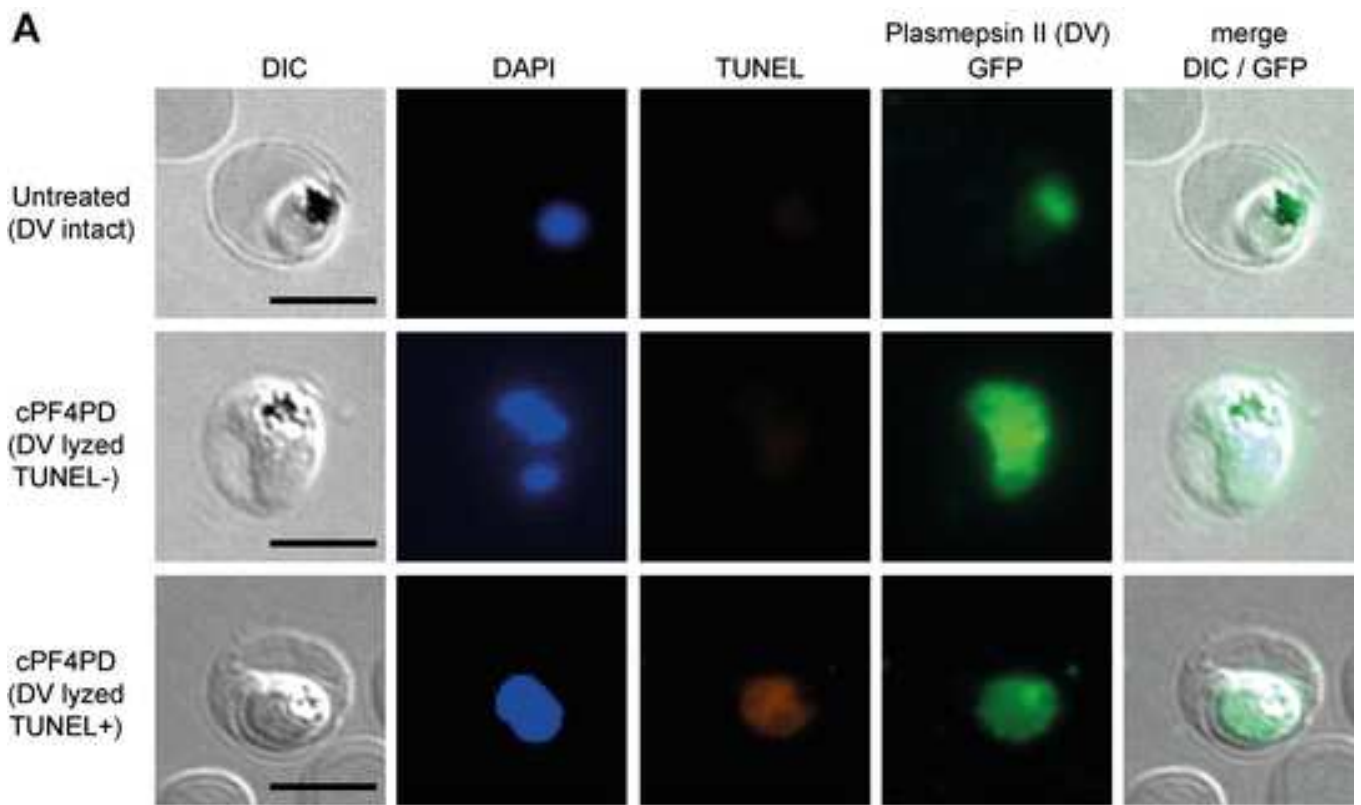


Figure 4

[Click here to download Figure Figure 4_s.tif](#)



KEY RESOURCES TABLE

REAGENT or RESOURCE	SOURCE	IDENTIFIER
Antibodies		
Goat Anti-Chicken IgY H&L (Alexa Fluor® 488)	Abcam	Cat# ab150169
Chicken Anti-GFP antibody	Abcam	Cat# ab13970
Streptavidin, Alexa Fluor™ 594 conjugate	Invitrogen	Cat# S11227
Bromodeoxyuridine/BrdU Antibody [Biotin]	Novus Biologicals	Cat# NB500-235B
Goat anti-Rabbit IgG (H+L) Cross-Adsorbed Secondary Antibody, DyLight 650	Invitrogen	Cat# SA5-10034
Rabbit Anti-Plasmodium falciparum Exp2	P. Gilson, Burnet Institute, Australia	N/A
Bacterial and Virus Strains		
Biological Samples		
Human O+ red blood cells	Australian Red Cross Blood Service (from adult donors aged 18-60 y)	N/A
Human O+ serum	Australian Red Cross Blood Service (from adult donors aged 18-60 y)	N/A
Human red blood cells for hemolysis assays	Healthy volunteers UQ (from adult donors aged 25-50 y)	N/A
Human serum from human male AB plasma (for peptide stability studies)	Sigma	Cat # H4522
Chemicals, Peptides, and Recombinant Proteins		
Alexafluor 488 hydroxylamine dye	ThermoFisher	Cat# A30629
1-palmitoyl-2-oleoyl- <i>sn</i> -glycero-3-phosphocholine (POPC)	Aussep (Avanti Polar Lipids)	Cat# 850457P
1-palmitoyl-2-oleoyl- <i>sn</i> -glycero-3-phospho-L-serine (POPS)	Aussep (Avanti Polar Lipids)	Cat# 840034P
1-palmitoyl-2-oleoyl- <i>sn</i> -glycero-3-phospho-(1'-rac-glycerol) (POPG)	Aussep (Avanti Polar Lipids)	Cat# 840457P
L- α -phosphatidylinositol	Aussep (Avanti Polar Lipids)	Cat# 840044P
N-oleoyl-D-erythro-sphingosylphosphorylcholine (sphingomyelin, SM)	Aussep (Avanti Polar Lipids)	Cat# 860587P
Cholesterol	Sigma	Cat# C8667
6-carboxyfluorescein (CF)	Sigma	Cat# C0662
Cytofix Fixation Buffer	BD Biosciences	Cat# 554655
Cytofix/Cytoperm Fixation/Permeabilization Solution	BD Biosciences	Cat# 554722
bisBenzimide H 33342 trihydrochloride	Sigma Aldrich	Cat# 14533
SlowFade® Gold Antifade Mountant with DAPI	Life Technologies	Cat# S36938
Recombinant human PF4	Peptotech	Cat# 300-16
PF4P ₁₋₃₅ >98% purity by HPLC (confirmed by MS)	Mimotopes	N/A
PF4P ₃₆₋₇₀ >98% purity by HPLC (confirmed by MS)	Mimotopes	N/A
2',7'-bis-(2-carboxyethyl)-5-(and-6)-carboxyfluorescein acetoxymethyl ester (BCECF-AM)	Molecular Probes, Thermo Fisher Scientific	Cat# B1170

Dextran, Fluorescein, 10,000 MW, Anionic	Molecular Probes, Thermo Fisher Scientific	Cat# D1821
Critical Commercial Assays		
Apo-BrdU Apoptosis Detection Kit	Jomar Life Research	Cat# 88-6671-88
Deposited Data N/A		
Experimental Models: Cell Lines N/A		
Experimental Models: Organisms/Strains		
<i>Plasmodium falciparum</i> , strain 3D7	R. Anders, La Trobe University, Australia	N/A
<i>Plasmodium falciparum</i> 3D7 PM2-GFP (expressing GFP-tagged Plasmepsin II)	Klonis et al., 2007	N/A
Oligonucleotides N/A		
Recombinant DNA N/A		
Software and Algorithms N/A		
Other		

1
2
3
4 **Defense peptides engineered from human platelet factor 4 kill *Plasmodium* by**
5 **selective membrane disruption**
6
7
8
9

10
11 Nicole Lawrence¹, Adelaide S M Dennis², Adele M Lehane², Anna Ehmann³, Peta J
12 Harvey¹, Aurélie H Benfield¹, Olivier Cheneval¹, Sónia Troeira Henriques^{1*}, David J
13 Craik^{1*} and Brendan J McMorran^{3,4*}
14
15
16
17
18

19 ¹ Institute for Molecular Bioscience, The University of Queensland, Brisbane, Qld, 4072,
20 Australia
21

22 ² Research School of Biology, The Australian National University, Canberra, ACT, 2600,
23 Australia
24

25 ³ The John Curtin School of Medical Research, The Australian National University,
26 Canberra, ACT, 2600, Australia
27

28 ⁴ Lead Contact
29

30 * Correspondence
31
32

33
34
35
36
37
38
39
40
41 brendan.mcmorran@anu.edu.au

42
43 s.henriques@imb.uq.edu.au

44
45
46 d.craik@imb.uq.edu.au
47
48
49
50
51
52
53
54
55
56
57
58
59
60
61
62
63
64
65

1
2
3
4
5
6
7
8
9
10
11
12
13
14
15
16
17
18
19
20
21
22
23
24
25
26
27
28
29
30
31
32
33
34
35
36
37
38
39
40
41
42
43
44
45
46
47
48
49
50
51
52
53
54
55
56
57
58
59
60
61
62
63
64
65

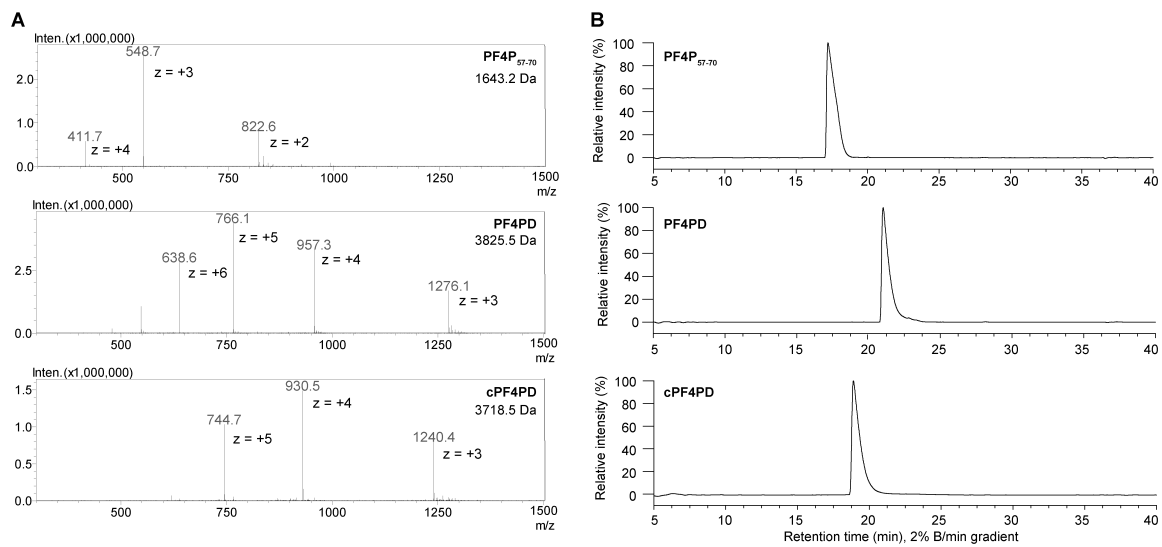


Figure S1. Analytical analysis of synthesized peptides. Related to STAR Methods and Table S1. A. ESI-MS trace with m/z indicating peptide size and purity. Correct peptide mass was determined by dissolving ~ 0.1 mg peptide in solvent A and running on ESI-MS. Peptide mass was determined using the formula: $mass = (m/z \cdot z) - z$, where z is the charge of the ion; **B.** Analytical HPLC trace showing peptide purity and retention time. Peptide purity was determined by dissolving ~ 0.1 mg of each peptide in solvent A (0.1% formic acid) and running a 2% B/min gradient (solvent B, 90% acetonitrile, 0.1% formic acid), starting from 1% solvent A.

1
2
3
4
5
6
7
8
9
10
11
12
13
14
15
16
17
18
19
20
21
22
23
24
25
26
27
28
29
30
31
32
33
34
35
36
37
38
39
40
41
42
43
44
45
46
47
48
49
50
51
52
53
54
55
56
57
58
59
60
61
62
63
64
65

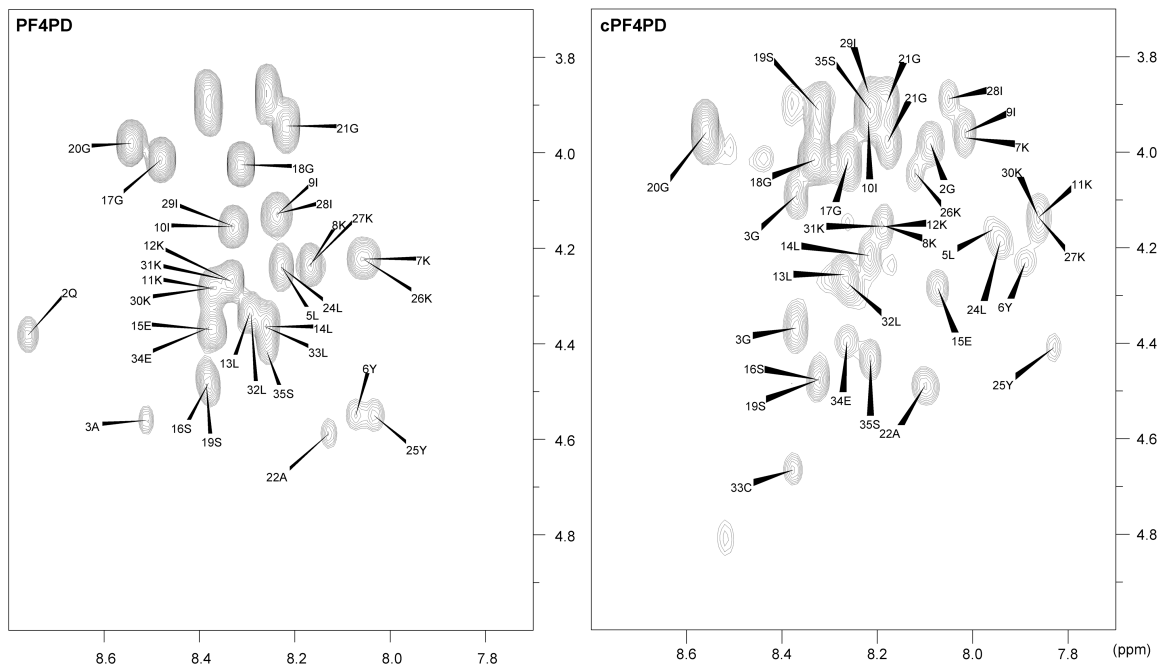


Figure S2. Two dimensional ^1H - ^1H TOCSY spectra of PF4PD and cPF4PD in 10% D₂O/ 90% H₂O. Related to STAR Methods. Expansion of H_N-H_α region with peaks annotated by residue and sequence number.

1
2
3
4
5
6
7
8
9
10
11
12
13
14
15
16
17
18
19
20
21
22
23
24
25
26
27
28
29
30
31
32
33
34
35
36
37
38
39
40
41
42
43
44
45
46
47
48
49
50
51
52
53
54
55
56
57
58
59
60
61
62
63
64
65

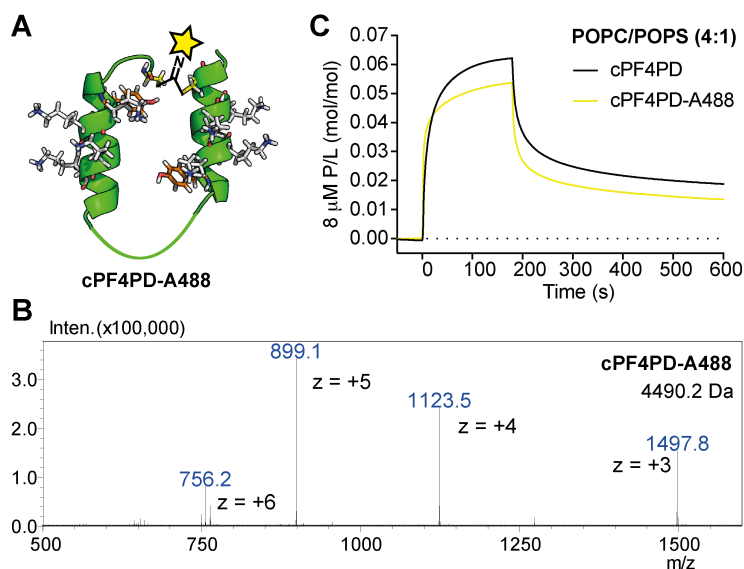
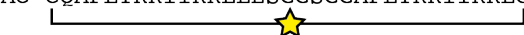


Figure S3. Labeling of cyclized PF4P dimer peptide with Alexa Fluor 488. Related to STAR Methods and Table S1. **A.** Cartoon showing the location of the A488 probe between Cys1 and Cys33, following dichloroacetone substitution of the peptide to produce a macrocyclic ketone, and subsequent oxime ligation of hydroxylamine-derivatized A488 onto the acetone linker; **B.** Correct mass of the peptide with a single A488 probe was confirmed with ESI-MS, see Table S1; **C.** Representative SPR sensorgrams showing similar association and dissociation of unlabeled and A488-labeled cPF4PD with POPC/POPS (4:1) model lipid bilayers.

Table S1. Primary sequence and characteristics of peptides derived from PF4. Related to Figure 1, Figure S1, Figure S3.

Peptide	Sequence	M _w ^a (Da)	Obs M _w ^b (Da)	ε ₂₈₀ ^c (M ⁻¹ cm ⁻¹)	RT ^d (min)
PF4P ₁₋₃₄	EAEEDGDLQCLCVKTTSQVRPRHITSLEVIKAGP	3724.2		0	
PF4P ₃₅₋₇₀	HCPTAQLIATLKNRKCICLDLQAPLYKKI IKKLLLES	4062.9	4062.9	1490	28.72
PF4P ₅₇₋₇₀	APLYKKI IKKLLLES*	1644.1	1643.2	1490	26.25
PF4PD	LQAPLYKKI IKKLLLESGGSGGAPLYKKI IKKLLLES*	3826.7	3825.5	2980	29.65
cPF4PD	CQAPLYKKI IKKLLLESGGSGGAPLYKKI IKKLLCES*	3720.6	3718.5	3105	26.67
cPF4PD-A488 ^e	Ac-CQAPLYKKI IKKLLLESGGSGGAPLYKKI IKKLLCES* 	4487.6	4490.2	3105	29.46

^a Average calculated mass from the amino acid sequence

^b Observed mass confirmed from m/z using ESI-MS, see Figure S1

^c Coefficient extinction at 280 nm (ε₂₈₀) calculated based on contribution of Tyr and Trp residues, and disulfide bonds

^d Retention time (RT) was determined using analytical RP-HPLC with a 1% solvent B/min gradient (solvent A, 0.1% TFA; solvent B, 90% ACN, 0.1% TFA)

^e A single A488 probe was attached to the peptide via oxime ligation of an acetone linkage between the cysteines, see Figure S3

Ac- denotes acetylated N terminus

* denotes amidated C terminus

Table S2. Helicity of PF4 peptides determined from circular dichroism (CD). Related to Figure 2.

Peptide	Total aa	aa predicted in helix ^a	Aqueous ^c		Aq/TFE ^d (1:1)	
			% helicity ^b	Helical residues	% helicity ^b	Helical residues
PF4P ₃₅₋₇₀	36	11	21	8	77	27
PF4P ₅₇₋₇₀	14	11	12	2	36	5
PF4PD	35	22	20	7	63	22
cPF4PD	35	22	52	18	63	22

^a Predicted from the relative number of residues expected to contribute to an α -helix, based on the structure of PF4 (PDB:1F9Q)

^b % helicity as calculated from CD spectra using the formula, $H_{\alpha} = (\theta_{222nm} - \theta_C) / (\theta_{222nm}^{\infty} - \theta_C)$, where θ_{222nm} is the lowest value between 218 and 222nm, $\theta_C = 2220 - 53T$ and $\theta_{222nm}^{\infty} = (-44000 + 250T)(1 - k / N_{res})$ with T in °C and k=3.0. [$\theta = mdeg / (c \cdot l \cdot N_{res})$, where *mdeg* is the CD output in millidegrees, *c* is the molar peptide concentration, *l* is the light path length in mm and N_{res} is the number of amino acid residues]

^c Aqueous solution is 100 mM NaF, 10 mM KH₂PO₄ pH 7.5

^d Inclusion (1:1 vol/vol) of trifluoroethanolamine (TFE) promotes α -helix formation for peptides that are able to achieve helical structure

Inventory of Supplemental Information

Figure S1. Analytical analysis of synthesized peptides.

Figure S2. Two dimensional ^1H - ^1H TOCSY spectra of PF4PD and cPF4PD in 10% D_2O /90% H_2O .

Figure S3. Labeling of cyclized PF4P dimer peptide with Alexa Fluor 488.

Table S1. Primary sequence and characteristics of peptides derived from PF4.

Table S2. Helicity of PF4 peptides determined from circular dichroism (CD).